
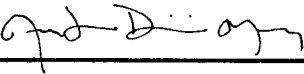


1. Classificação <i>INPE-COM.2/NTI</i>		2. Período <i>agosto de 1975</i>	4. Critério de Distribuição:
3. Palavras Chave (selecionadas pelo autor) <i>BAROCLINIC INSTABILITY, QUASI-GEOSTROPHIC, EFFECTS OF CURVATURE, EDDY FLUXES, PARAMETERIZATION</i>			interna <input checked="" type="checkbox"/> externa <input type="checkbox"/>
5. Relatório nº <i>INPE-736-NTI/029</i>	6. Data <i>9 de setembro de 1975</i>	7. Revisado por - <i>Peter H. Stone*</i>	
8. Título e Sub-Título <i>CURVATURE EFFECTS ON BAROCLINIC INSTABILITY</i>		9. Autorizado por -  <i>Walter D. Gonzales A.</i>	
10. Setor <i>CEA</i>	Código <i>4.01</i>	11. Nº de cópias <i>3</i>	
12. Autoria <i>Antonio Divino Moura e Peter H. Stone*</i>		14. Nº de páginas <i>48</i>	
13. Assinatura Responsável 		15. Preço	
16. Sumário/Notas <p><i>A baroclinic stability analysis is performed for a simple family of zonal shear profiles over a sphere, using a two-layer, quasi-geostrophic model. The stability properties and the structure of the most unstable waves are qualitatively similar to those on a β-plane. However, curvature effects play a major role in locating some of the important features of the most unstable waves. In particular, the locations of the maximum wave amplitude, maximum eddy heat fluxes, and maximum convergence of the eddy angular momentum flux are all well correlated with the location of the maximum excess of the vertical shear over the minimum value necessary for local instability on a sphere. Consequently the eddy momentum flux tends to generate a mid-latitude jet even if there is no pre-existing mid latitude jet in the basic state zonal flow. These findings suggest the elements needed for parameterizing the meridional variations of baroclinic eddy fluxes accurately.</i></p>			
17. Observações <i>Submetido para publicação no Journal of Atmospheric Sciences em agosto de 1975 (pelo M.I.T.).</i>			
* <i>Massachusetts Institute of Technology.</i>			

"CURVATURE EFFECTS ON BAROCLINIC INSTABILITY"

Antonio D. Moura ¹ and Peter H. Stone

Department of Meteorology

Massachusetts Institute of Technology

Cambridge, MA 02139

August, 1975

(submitted to the Journal of Atmospheric Sciences)

¹ On leave from and presently at: Instituto de Pesquisas Espaciais
12.200 -São José dos Campos, SP, Brazil

ABSTRACT

A baroclinic stability analysis is performed for a simple family of zonal shear profiles over a sphere, using a two-layer, quasi-geostrophic model. The stability properties and the structure of the most unstable waves are qualitatively similar to those on a β - plane. However, curvature effects play a major role in locating some of the important features of the most unstable waves. In particular, the locations of the maximum wave amplitude, maximum eddy heat fluxes, and maximum convergence of the eddy angular momentum flux are all well correlated with the location of the maximum excess of the vertical shear over the minimum value necessary for local instability on a sphere. Consequently the eddy momentum flux tends to generate a mid latitude jet even if there is no pre-existing mid latitude jet in the basic state zonal flow. These findings suggest the elements needed for parameterizing the meridional variations of baroclinic eddy fluxes accurately.

1. Introduction

It has been suggested (Stone, 1974) that the Earth's curvature might strongly affect the detailed meridional distribution of heat and momentum transports by baroclinic eddies. These curvature effects, which are not captured in a simple β - plane analysis, may have to be included for a correct formulation of heat and momentum transports by baroclinic eddies and their parameterization in atmospheric models.

In this work we examine the effects of curvature on the heat and momentum transports and on the meridional structure of the most unstable baroclinic mode. We make use of a two-layer, quasi-geostrophic model on a sphere and study the stability properties of a family of basic zonal wind profiles. By varying the parameters in the family of profiles, we are able to draw conclusions about the parameter dependence of the eigenfunctions' latitudinal structure and the momentum and heat transports by the baroclinic eddies. We compare our solutions with the results of two-layer, quasi-geostrophic investigations on a β - plane (Phillips, 1954; Pedlosky, 1964.a, 1964.b; Stone, 1969, 1974; Simmons, 1974).

Recently Hollingsworth (1975) has also presented a study of the curvature effects using the same model as ours. His results are confined to a basic state wind profile which varies as the cosine of the latitude. Our results for such a wind profile are in good agreement with Hollingsworth's, taking into account the somewhat different parameter values used in the two studies. In addition our study includes results for a large number of wind profiles with different latitudinal variations, and this has allowed us to draw a number of conclusions not possible in Hollingsworth's study.

2. The Mathematical Model

We describe the unstable baroclinic waves by means of a linearized, quasi-geostrophic two-level model on a sphere. The appropriate equations have been given by Moura (1975) (his Eqs. (6.23) - (6.26) with the parameter $\gamma = 0$). The quasi-geostrophic approximation formally breaks down near the equator; but Moura (1975) showed that the unstable solutions obtained using the balance equations do not differ significantly from those obtained using the quasi-geostrophic equations, because the most unstable wave amplitudes in low latitudes are small.

In our study we will use for the basic state zonal wind profile the family given by $\bar{u}(\mu, p) = a \alpha(p) (1 - \mu^2)^{1/2} (1 + \delta \mu^2)$, where a is the earth's radius, $\alpha(p)$ is a function of pressure, p , given at two levels, μ is $\sin(\text{latitude})$, and δ is a parameter describing the meridional shear. The profile with $\delta = 0$ is a simple $\cos(\text{lat})$ profile, and is analogous to a profile on a β -plane with no meridional shear. All the solutions we will discuss are barotropically stable (see Appendix A).

We seek solutions of the equations in the form:

$$\begin{pmatrix} \psi \\ \theta \\ \chi \\ \tau \end{pmatrix} = \text{Re} \left\{ \exp(i s \phi - i \omega s t') \sum_{n=s}^N P_n^s(\mu) \begin{pmatrix} \psi_n^s(t') \\ \theta_n^s(t') \\ i \chi_n^s(t') \\ T_n^s(t') \end{pmatrix} \right\} \quad (2.1)$$

with $s=1, 2, 3, \dots$

Where χ = velocity potential at level 1 (upper level).

$\theta = (\psi_1' - \psi_3')/2$, difference between the streamfunctions at the upper level (1) and lower level (3).

$\Psi = (\Psi_1 + \Psi_3)/2$, mean streamfunction.

$\tau = (\phi_1 - \phi_3)/4\Omega$, difference between the geopotential at levels 1 and 3;

Ω is the Earth's rate of rotation.

s = zonal wave number.

$t' = 2\Omega t$; t is time.

$\omega = (\alpha_1 + \alpha_3)/4\Omega$; $\Lambda = (\alpha_1 - \alpha_3)/4\Omega$

$P_n^s(\mu)$ = associated Legendre "polynomial".

We then use (2.1) in Moura's Eqs. (6.23)-(6.26), together with the properties of $P_n^s(\mu)$. (Korn & Korn, p.870), to get:

$$\dot{\Psi}_n^s = b_n \Psi_{n-2}^s + a_n \Psi_n^s + c_n \Psi_{n+2}^s + e_n \Theta_{n-2}^s + d_n \Theta_n^s + f_n \Theta_{n+2}^s \quad (2.2)$$

$$\dot{\Theta}_n^s = b_n \Theta_{n-2}^s + a_n \Theta_n^s + c_n \Theta_{n+2}^s + e_n \Psi_{n-2}^s + d_n \Psi_n^s + f_n \Psi_{n+2}^s + g_n X_{n-1}^s + h_n X_{n+1}^s \quad (2.3)$$

$$\dot{T}_n^s = j_n T_{n-2}^s + i_n T_n^s + k_n T_{n+2}^s + \ell_n \Psi_{n-3}^s + p_n \Psi_{n-1}^s + q_n \Psi_{n+1}^s + r_n \Psi_{n+3}^s + s_n X_n^s \quad (2.4)$$

$$T_n^s = g_n \Theta_{n-1}^s + h_n \Theta_{n+1}^s \quad (2.5)$$

where $(\dot{}) \equiv \frac{\partial}{\partial t'}$. Appendix B gives the coefficients a_n, b_n, \dots etc. as well as a discussion of the numerical solution of the problem.

T_n^S is eliminated from (2.4) by means of (2.5), which result is used to substitute for X_{n-1}^S and X_{n+1}^S in (2.3). A matrix equation is obtained in the form of $\underline{A}\dot{\underline{Y}} = \underline{B}\underline{Y}$, where the matrices \underline{A} and \underline{B} are given in Appendix B. To solve this matrix equation we take the inverse of \underline{A} and write $\dot{\underline{Y}} = \underline{A}^{-1}\underline{B}\underline{Y}$. The solution is obtained with $\underline{Y}(t') = \exp(-i\sigma t') \underline{X}$, by solving the ordinary eigenvalue-eigenfunction problem:

$$(\underline{A}^{-1}\underline{B} - \sigma\underline{I}) \underline{X} = 0 \quad (2.6)$$

We then look for solutions for $\sigma = \lambda + i\nu$ with maximized growth rates with respect to the zonal wave number (s), mean meridional wave number (m), and symmetry, for fixed values of ω , Λ , and S . m is defined as one plus the number of zeros in the real part of ψ' , between the equator and the pole. S measures the static stability and is defined by

$$S = (2)^{1/\gamma} \frac{R}{16\Omega^2 a^2} (\theta_{s1} - \theta_{s2}), \quad (2.7)$$

where γ is the ratio of specific heats, R is the gas constant, and θ_s is the basic state potential temperature. In all our solutions we will choose $\alpha_3 = 0$ so that $\omega \equiv \Lambda$. Consequently our solutions for the most unstable modes will be functions of three independent parameters, the vertical shear, Λ , the horizontal shear, δ , and the static stability, S .

Figs. 1 and 2 show the shear profiles, $\bar{u}_1 - \bar{u}_3$ vs. latitude, used for our calculations far from and near neutral stability, respectively. These figures also show the observed mean annual values of \bar{u} at 200 mb minus \bar{u} at 700 mb, as given by Oort and Rasmusson (1971), and the minimum shear necessary on a β - plane for a profile with no meridional shear to be baroclinically unstable - namely, $\bar{u}_1 - \bar{u}_3 = 4\Omega a S \cos(\text{lat}) / \sin^2(\text{lat})$ (Phillips, 1954, Pedlosky, 1964a).

This minimum shear was calculated using $S = 0.0050$, which is the annual mean tropospheric value of S calculated from Oort and Rasmusson's (1971) data. Horizontal shear in the basic state zonal flow does not seem to affect this stability criterion significantly (Pedlosky, 1964b, Stone, 1969) - i.e., the flow on a β - plane is stable if and only if the shear profile is less than the critical shear everywhere. Our results showed that this criterion also seems to work quite well on a sphere, if the critical shear is taken to be a function of latitude- i.e., the flow is stable if and only if the shear is less than the local value of the critical shear at all latitudes. It is interesting to note that the mean annual shear for the atmosphere coincides with the local values of the critical shear within the error of the observations, from 38°N up to 75°N (no observations are available further north).

Profiles 2 to 4 in Fig. 2 differ from the similarly numbered profiles in Fig. 1 only in the respective values of Λ . Profiles 2, 3, and 5 in Fig. 1 have maximum shear approximately equal to the observed maximum shear, but their maxima are at different latitudes. These profiles all exceed the critical shear for instability in high latitudes, but fall short of it in low latitudes. Profile 4 however exceeds the critical shear only in mid-latitudes. Profiles 2 and 3 in Fig. 2 exceed the critical shear only in polar latitudes, but by very small amounts. Profile 4 in Fig. 2 falls short of the critical shear at all latitudes, but approaches it very closely in mid-latitudes. Nevertheless this profile was found to be very slightly unstable, which merely emphasizes that the stability criterion given above is only an approximate one for non-uniform flow on a sphere.

3. Results

We will now discuss the numerical solutions corresponding to the profiles illustrated in Figs. 1 and 2. These solutions are displayed in Figs. 3 - 9.

More details of the solution for profile 2 in Fig. 1 have been given by Moura (1975). Part a of each Figure shows the amplitude and phase of the most unstable geopotential eigenfunction at levels 1 and 3 for the profile cited. Part b shows the corresponding angular momentum transports and horizontal and vertical heat transports. For all the figures, the functions have been computed at every 2° of latitude.

The Geopotential Eigenfunctions ϕ_1' and ϕ_3'

The amplitude of the eigenfunctions ϕ_1' and ϕ_3' has two distinct behaviors depending on whether the basic zonal profile is near or far from neutral stability. In the latter case (part a of Figs. 3,5,7,9), the amplitudes are smooth functions of latitude, resembling the solutions found by Simmons (1974), with maxima in middle or high latitudes. In the former case (part a of Figs. 4,6,8; near the instability threshold), the amplitudes oscillate rapidly between the equator and the pole, in agreement with Stone's (1969) study. Especially in the upper layer, they penetrate further into low latitudes than do those for the more unstable profiles of \bar{U} . In almost all cases there seems to exist a strong correlation between the location of the maximum of the amplitude of ϕ_1' and the latitude where the local instability is greatest (i.e., where $4\Omega a \Lambda \cos(\text{lat}) \{1 + \delta \sin^2(\text{lat}) - \frac{S}{\Lambda} \sin^{-2}(\text{lat})\}$ is largest, for the family of profiles used). The peak amplitude of ϕ_3' tends to occur very near the peak amplitude of ϕ_1' , but usually a few degrees of latitude poleward of it. Table 1 summarizes these correlations. There is a notable exception for the profile 4 in Fig. 2, probably because the local stability in this case is nearly uniform over a wide range of latitudes. The eigenfunctions for this marginal case (shown in Fig. 8a) for levels 1 and 3 peak at 30°N and 69°N respectively.

In all β - plane analyses, the amplitudes peak near where the vertical shear of the zonal velocity is a maximum. The simple baroclinic criterion in this case is a constant (because $\cos(\text{lat.})$ and $\sin^2(\text{lat.})$ are evaluated at the coordinate origin). For a symmetric \bar{U} profile, on a β - plane, the (constant) criterion is therefore automatically exceeded most at the location of maximum vertical shear of the zonal wind. The inclusion of curvature (e.g., the complete variability of f) in our spherical analysis makes a clear distinction between the location of maximum shear and the location of maximum excess of shear over the local criterion, allowing for the proper physical conclusion to be drawn.

Angular Momentum Flux

The momentum transport by baroclinic eddies in the β - plane analyses is always against the latitudinal gradient of the basic zonal wind profile, changing sign where the profile is a maximum. This has led to the conclusion that the baroclinic eddies, although not explaining the formation of jets, are able to maintain a pre-existing jet structure of the basic zonal flow (Pedlosky, 1964.b; Stone, 1969; Simmons, 1974).

The curvature effects lead to quite a different conclusion. The angular momentum transports are polewards everywhere for all the profiles with the exception of profile 4 for which there is a reversal of sign (see Figs. 3b-9b). For all of the profiles, angular momentum is transported away from where the zonal velocity is a maximum to higher latitudes. For the profile 4 ($\bar{U} \propto \cos^3(\text{lat.})$) there exists a tendency for jet formation at approximately 45°N (Fig. 7.b) and 30°N (Fig. 8.b) for the solutions far from neutral stability and near neutral stability, respectively. However, there is a strong correlation between the location of the maximum convergence of angular momentum flux and the latitude where the local

instability is a maximum. Table I shows the specific locations for the profiles used. Consequently one would expect baroclinic eddies to shift any pre-existing jet towards the position of maximum local instability.

Horizontal and Vertical Heat Transports

The latitudinal distributions of horizontal and vertical eddy heat transports look much alike; i.e., upward (downward) heat transport coinciding with poleward (equatorward) horizontal eddy heat transport, with peaks at the same latitude. Stone (1974) noted this property for cases near neutral stability, and our results indicate that it also holds far from neutral stability. For all the cases near neutral stability there is a sign reversal of heat transports, located equatorward of the maximum heat transport (see Figs. 4.b, 6.b, 8b). This sign reversal does not seem to occur for the solutions very far from neutral stability (see Figs. 5.b, 9.b), although it does still occur for the solutions moderately far from neutral stability (see Figs. 3.b, 7.b). The location of this sign reversal appears well correlated with the latitude where the curve of the local criterion for stability intercepts the curves of basic zonal wind profiles. Again, profile 4 in Fig. 2 is an obvious exception to this correlation. This correlation is summarized in Table I, and seems to reinforce the conclusion reached by Stone (1974) that "...to a first approximation the heat flux is equatorward in regions where the local criterion for stability is satisfied, and poleward in regions where it is not."

The locations of maximum poleward heat transport are well correlated with the location where the local instability of the basic state is largest (see Table I). These locations are even better correlated with the locations of maximum convergence of angular momentum (Table I). This fact should be taken into account in any study aiming at a correct parameterization of heat transports by the baroclinic eddies. Curvature effects are very important in this respect (i.e., in locating the transport

maxima), and neglecting them appears to have been responsible for the defective location of this maximum in Stone's (1974) parameterization of the meridional variation of eddy heat fluxes by baroclinic waves. The curvature effects displace the maxima poleward of the maxima in the basic state wind profile.

Meridional Scale of Baroclinic Waves

Here we shall consider the question of the meridional scale of the most unstable baroclinic wave on a globe. Stone (1969) addressed this question with an analysis (on a β -plane) for unstable waves near the baroclinic stability threshold, concluding that the waves have their own internal meridional scale, given by the radius of deformation. His definition of the mean meridional scale is the mean separation of the zeros in the real part of the complex streamfunction in the upper layer, between the equator and the pole. In Figs. 3.a - 9.a, this number of zeros plus 1 is given by m (e.g., $m=3$ in Fig. 3.a).

In a recent numerical study, Simmons (1974) found that there are also some solutions (far from neutral stability) for which the dominant scale is not the radius of deformation. Guided by his numerical solutions, he obtained an analytic formulation for a parabolic profile, valid for baroclinic waves far from neutral stability. The amplitudes of the streamfunctions have a Gaussian behavior with latitude, centered at the position where the zonal profile is a maximum. These amplitude functions have meridional scales given by the geometric mean of the radius of deformation and the distance from the equator to pole.

In an attempt to verify the existence of these two scales, when curvature effects are included, we have derived solutions (Figs. 10 - 12) for three additional cases, in which the radius of deformation is just half the value used in three of the solutions discussed earlier (Figs. 9, 7, and 6). To accomplish this, we decreased S by a factor of 4, but kept

the ratio S/Λ constant (i.e., the latitudinal shape of $4\Omega a \Lambda \cos(1at) [1 + \delta \sin^2(1at) - (S/\Lambda) \sin^{-2}(1at)]$ is the same in each comparison.) The results of these additional cases have also been included in Table I, and they verify the conclusions reached above concerning the correlation of the local stability criterion with the properties of the dominant eigenfunctions and their eddy fluxes.

Fig. 9a shows $S = 3$ and $m = 4$, while its counterpart, Fig. 12a, shows $S = 7$ and $m = 10$. The width of the region in which the amplitude of ϕ_1 exceeds half its maximum value decreases by a factor of 1.36 from Fig. 9a to Fig. 12a. Fig. 7a shows $S = 5$ and $m = 2$, while its counterpart, Fig. 11a, shows $S = 11$ and $m = 3$. In this case the half-amplitude width decreases by a factor of 1.67. These two pairs of solutions are far from neutral stability. For the other pair, which is near neutral stability, Fig. 6a shows $S = 2$ and $m = 5$, while Fig. 10a shows $S = 4$ and $m = 11$. In this case the half-width of the amplitude function is not well defined.

In all three cases the value of S is approximately doubled, in accord with the β - plane results showing that the zonal scale is proportional to the radius of deformation (Phillips, 1954). The values of m are also roughly doubled, implying that the mean meridional wave scale is also proportional to the radius of deformation, in accord with Stone's (1969) results. On the other hand far from neutral stability the half-amplitude width varies roughly like the square root of the radius of deformation, in accord with Simmons' (1974) results. The behavior of the eigenfunctions leads one to conclude that the dominant meridional scale is the mean wave scale near neutral stability, but becomes the half-amplitude width far from neutral stability, with a corresponding change in the dependence of the dominant scale on the radius of deformation.

4 Conclusions

Our results show that the baroclinic stability problem in many respects is not modified by curvature effects. The baroclinic stability criterion on a β - plane still holds to a good approximation on a sphere, provided that it is applied locally; the most unstable zonal wave-length is still proportional to the radius of deformation; the unstable baroclinic waves near neutral stability still have amplitudes which oscillate rapidly between the equator and the pole, with a characteristic scale roughly proportional to the radius of deformation; and the unstable waves far from neutral stability still have amplitudes which exhibit a quasi-Gaussian behavior with latitude, with characteristic scale roughly proportional to the square - root of the radius of deformation.

Of the various basic state wind profiles which we studied, the one which seems to give the most realistic results for the structure of the unstable waves is profile 4 in Fig. 1. This profile does approximate the observed profile in mid-latitudes (see Fig. 1). The eddy fluxes generated by the dominant unstable wave accompanying this profile (see Fig. 7b) closely resemble the observed fluxes due to transient eddies (Oort and Rasmusson, 1971). For example, there is a poleward flux of momentum in low latitudes and an equatorward flux in high latitudes, with the former being much stronger; and there is a relatively small equatorward flux of heat in very low latitudes. The eigenfunctions in this case also illustrate the most important difference between the unstable waves on a sphere and those on a β - plane, i.e., the eddy momentum flux generated on a sphere tends to create a mid-latitude jet, even though there is no pre-existing mid-latitude jet in the basic state wind profile.

Our results also establish the importance of the local stability criterion on a sphere in determining the detailed meridional structure of unstable baroclinic waves. There is a strong correlation between the location of maximum local instability and the locations of maximum wave amplitude, maximum eddy momentum

flux convergence, maximum poleward eddy heat transport, and maximum upward eddy heat transport. The meridional and vertical eddy heat transports are closely correlated and tend to change sign on the equatorward side of their maxima, at the location where the local instability first vanishes. Any parameterization of the meridional variation of the eddy fluxes should take these properties into account.

ACKNOWLEDGEMENTS

This research was supported in part by the National Aeronautics and Space Administration under Grant NGR 22-009-727, in part by Instituto de Pesquisas Espaciais (CNPq/ INPE), Brazil and in part by the National Science Foundation under Grant GA 28724.

Appendix A

Barotropic Stability of the Model

The energy equation for our model shows that there is a possibility for barotropic instability as well as for baroclinic instability. To study under what conditions barotropic instability may be present, we derive from the vorticity equation (Moura's (1975) Eq. 6.23 with $\gamma = 0$) the necessary criterion for instability analogous to that first found by Lord Rayleigh (1880). With no vertical shear ($\Lambda = 0$), the resulting criterion for our family of profiles is

$$\int_{-1}^{+1} a(\mu) |\psi|^2 \frac{d}{d\mu} [\mu + 2\omega\mu(1 - \delta + 2\delta\mu^2)] d\mu = 0 \quad (\text{A.1})$$

where

$$a(\mu) = s\nu / \{v^2 [\lambda - s\omega(1 + \delta\mu^2)]^2\}$$

We thus conclude that the necessary condition for barotropic instability is that $\frac{d}{d\mu} [\mu + 2\omega\mu(1 - \delta + 2\delta\mu^2)]$ change sign between $\mu = -1$ and $\mu = +1$. This is the same result obtained in a β - plane analysis, i.e., that the derivative of the total vorticity has to change sign between the boundaries for instability.

For all the profiles used in our study this criterion is not satisfied. Therefore, all the profiles we studied are barotropically stable.

Appendix B

Numerical Solution of the Matrix Equation $A\dot{Y} = BY$

The coefficients appearing in (2.2) - (2.5) are:

$$a_n = s \left[\frac{(-1-2\omega(1-\delta))}{(n(n+1))} + \frac{\delta \omega (1-12/(n(n+1)))((n-s+1)(n+s+1))}{((2n+1)(2n+3)) + (n-s)(n+s)/((2n-1)(2n+1))} \right]$$

$$b_n = \delta \omega s \left(\frac{(n-2)(n-1)-12}{(n(n+1))} \right) \left(\frac{(n-s-1)(n-s)}{(2n-3)(2n-1)} \right)$$

$$c_n = \delta \omega s \left(\frac{(n+2)(n+3)-12}{(n(n+1))} \right) \left(\frac{(n+s+1)(n+s+2)}{(2n+3)(2n+5)} \right)$$

$$d_n = \Delta s \left[\frac{1-2(1-\delta)}{(n(n+1))} + \frac{\delta (1-12/(n(n+1)))((n-s+1)(n+s+1))}{((2n+1)(2n+3)) + (n-s)(n+s)/((2n-1)(2n+1))} \right]$$

$$e_n = \frac{\Delta}{\omega} b_n$$

$$f_n = \frac{\Delta}{\omega} c_n$$

$$g_n = \frac{(n-1)(n-s)}{(n(2n-1))}$$

$$h_n = \frac{(n+2)(n+s+1)}{(n+1)(2n+3)}$$

$$i_n = \delta \omega s \left(\frac{(n-s+1)(n+s+1)}{(2n+1)(2n+3)} + \frac{(n-s)(n+s)}{(2n-1)(2n+1)} \right)$$

$$j_n = \delta \omega s \left(\frac{(n-s-1)(n-s)}{(2n-3)(2n-1)} \right)$$

$$k_n = \delta \omega s \left(\frac{(n+s+1)(n+s+2)}{(2n+3)(2n+5)} \right)$$

$$l_n = -\delta \Delta s \left(\frac{(n-s-2)(n-s-1)(n-5)}{(2n-5)(2n-3)(2n-1)} \right)$$

$$p_n = -\Lambda s \left[(n-s)/(2n-1) + 6((n-s)(n-s+1)(n+s+1)/((2n-1)(2n+1)(2n+3)) + \right. \\ \left. (n-s)^2(n+s)/((2n-1)^2(2n+1)) + (n-s-1)(n-s)(n+s+1)/ \right. \\ \left. (2n-3)(2n-1)^2) \right]$$

$$q_n = -\Lambda s \left[(n+s+1)/(2n+3) + \delta((n-s+2)(n+s+1)(n+s+2)/((2n+3)^2(2n+5)) + \right. \\ \left. (n-s+1)(n+s+1)^2/((2n+1)(2n+3)^2) + (n-s)(n+s)(n+s+1)/ \right. \\ \left. (2n-1)(2n+1)(2n+3)) \right]$$

$$r_n = -\delta \Lambda s ((n+s+1)(n+s+2)(n+s+3)/((2n+3)(2n+5)(2n+7)))$$

$$s_n = -S n(n+1)$$

where S is the non-dimensional static stability and $\Lambda = (\alpha_1 - \alpha_3)/4$ is a measure of the vertical shear.

When T_n^S is eliminated between (2.4) and (2.5) and the resulting equation used to substitute for X_{n-1}^S and X_{n+1}^S , we obtain:

$$-t_n g_{n-1} \dot{\Theta}_{n-2}^S + (1-t_n h_{n-1} - u_n g_{n+1}) \dot{\Theta}_n^S - u_n h_{n+1} \dot{\Theta}_{n+2}^S = -t_n j_{n-1} g_{n-3} \Theta_{n-4}^S \\ + (b_n - t_n (j_{n-1} h_{n-3} + i_{n-1} g_{n-1}) - u_n j_{n+1} g_{n-1}) \Theta_{n-2}^S + (a_n - t_n (k_{n-1} g_{n+1} + \\ h_{n-1} i_{n-1}) - u_n (j_{n+1} h_{n-1} + i_{n+1} g_{n+1})) \Theta_n^S + (c_n - t_n (k_{n-1} h_{n+1} - u_n (k_{n+1} g_{n+3} + \\ i_{n+1} h_{n+1}))) \Theta_{n+2}^S - u_n k_{n+1} h_{n+3} \Theta_{n+4}^S - t_n l_{n-1} \Psi_{n-4}^S + (e_n - t_n (p_{n-1} - u_n l_{n+1})) \Psi_{n-2}^S \\ + (d_n - t_n (q_{n-1} - u_n p_{n+1})) \Psi_n^S + (f_n - t_n (r_{n-1} - u_n q_{n+1})) \Psi_{n+2}^S - u_n r_{n+1} \Psi_{n+4}^S$$

(B.1)

where $t_n = g_n / s_{n-1} = (n-s) / (S n^2 (2n-1))$; $t_s = 0$ for all s

$$u_n = h_n / s_{n+1} = -(n+s+1) / (S(n+1)^2 (2n+3))$$

Equations (B.1) and (2.2) can be written in matrix form as follows:

$$\underline{AY} = \underline{BY} \tag{B.2}$$

We then solve the eigenvalue problem (2.6) for σ with fixed values of S, ω, Λ, s . It is necessary to truncate the matrix $\underline{A}^{-1}\underline{B}$ in order to solve (2.6). The convergence of the most unstable root was obtained by comparing its value for matrices of sizes 30x30, 36x36, and 42x42. For the solutions far from neutral stability an agreement of 10^{-6} was obtained, while for the solutions near neutral stability the accuracy was better than 10^{-2} . In the latter case, the convergence is slower because the solutions oscillate more between $\mu=0$ and $\mu=1$. The convergence is also much slower for \bar{U} profiles which have a more complicated μ dependence than those we have studied.

The matrices $\underline{Y}, \underline{A}$ and \underline{B} appearing in (B.2) are:

$$\underline{Y} = \begin{pmatrix} \Theta_n^s \\ \Psi_n^s \\ \Theta_{n+2}^s \\ \Psi_{n+2}^s \\ \vdots \\ \Theta_{n+2k}^s \\ \Psi_{n+2k}^s \\ \vdots \\ \vdots \\ \vdots \end{pmatrix} ; n = s \quad \text{or} \quad n = s+1$$

$$\begin{bmatrix}
 (i-t_n h_{n-1} - u_n g_{n+1}) & (0) & \dots & \dots & \dots & (0) & \dots & \dots & \dots & 0 \\
 (0) & (1) & \dots & \dots & \dots & (0) & \dots & \dots & \dots & 0 \\
 -(t_{n+2} g_{n+1}) & (0) & \dots & \dots & \dots & (1-t_{n+2} h_{n+1} - u_{n+2} g_{n+3}) & (0) & \dots & \dots & (0) & \dots & \dots & 0 \\
 (0) & (0) & \dots & \dots & \dots & (0) & (1) & \dots & \dots & \dots & \dots & 0 \\
 (0) & (0) & \dots & \dots & \dots & (-t_{n+4} g_{n+3}) & (0) & (1-t_{n+4} h_{n+3} - u_{n+4} g_{n+5}) & (0) & \dots & \dots & \dots & 0 \\
 \vdots & \vdots & \dots & \dots & \dots & (0) & (0) & \dots & \dots & (1) & (0) & \dots & \dots \\
 \vdots & \vdots & \dots & \dots & \dots & \vdots & \vdots & \vdots & \vdots & \vdots & \vdots & \vdots & \vdots \\
 \vdots & \vdots & \dots & \dots & \dots & \vdots & \vdots & \vdots & \vdots & \vdots & \vdots & \vdots & \vdots \\
 \vdots & \vdots & \dots & \dots & \dots & \vdots & \vdots & \vdots & \vdots & \vdots & \vdots & \vdots & \vdots \\
 \vdots & \vdots & \dots & \dots & \dots & \vdots & \vdots & \vdots & \vdots & \vdots & \vdots & \vdots & \vdots \\
 0 & 0 & \dots & \dots & \dots & 0 & 0 & \dots & \dots & 0 & 0 & \dots & 0
 \end{bmatrix}$$

MATRIX \underline{A} (n=s or n+t+1)

$$\begin{pmatrix}
 [a_n - t_n(k_{n+1}g_{n+1} + i_{n+1}h_{n+1}) - \\ -u_n(j_{n+1}h_{n+1} + l_{n+1}g_{n+1})] & [d_n - t_n g_{n+1} - \\ -u_n p_{n+1}] & [c_n - t_n(k_{n+1}h_{n+1}) - \\ -u_n p_{n+1}] & [f_n - t_n r_{n+1} - \\ -u_n q_{n+1}] & [-u_n k_{n+1}h_{n+1}] [-u_n r_{n+1}] 0 \\
 [d_n] & [a_n] & [f_n] & [c_n] & [0] & \dots \\
 [b_{n+2} - t_{n+2}(j_{n+1}h_{n+1} + i_{n+1}g_{n+1}) - \\ -u_{n+2}(j_{n+3}h_{n+1} + i_{n+3}g_{n+1})] & [e_{n+2} - t_{n+2}p_{n+1} - \\ -u_{n+2}l_{n+3}] & [a_{n+2} - t_{n+2}(k_{n+1}g_{n+1} + i_{n+1}h_{n+1}) - \\ -u_{n+2}(j_{n+3}h_{n+1} + i_{n+3}g_{n+1})] & [d_{n+2} - t_{n+2}q_{n+1} - \\ -u_{n+2}p_{n+3}] & [c_{n+2} - \dots] & [f_{n+2} - \dots] \\
 [e_{n+2}] & [b_{n+2}] & [d_{n+2}] & [a_{n+2}] & [f_{n+2}] & [c_{n+2}] \\
 [-t_{n+4}j_{n+3}g_{n+3}] & [-t_{n+4}l_{n+3}] & [b_{n+4} - t_{n+4}(j_{n+3}h_{n+1} + i_{n+3}g_{n+1}) - \\ -u_{n+4}(j_{n+5}g_{n+1})] & [e_{n+4} - \dots] & [a_{n+4} - \dots] & [d_{n+4} - \dots] \\
 0 & \vdots & [e_{n+4}] & [b_{n+4}] & [d_{n+4}] & [a_{n+4}] \\
 \vdots & \vdots & [-t_{n+6}j_{n+5}g_{n+5}] & [---] & [---] & [---] \\
 \vdots & \vdots & 0 & 0 & [e_{n+6}] & \vdots \\
 \vdots & \vdots & \vdots & \vdots & \vdots & [---] \\
 \vdots & \vdots & 0 & 0 & 0 & 0 \\
 \vdots & \vdots & \vdots & \vdots & \vdots & \vdots \\
 0 & \vdots & \vdots & \vdots & \vdots & 0
 \end{pmatrix}$$

MATRIX B (n=s or n=s+1) Banded matrix with bandwidth 10.

REFERENCES

- HOLLINGSWORTH, A., 1975: Baroclinic Instability of a simple flow on the sphere. Q.J.Roy. Meteor. Soc., 101, 495-528.
- KORN & KORN, 1968: Mathematical Handbook for Scientists and Engineers. McGraw-Hill Book Co., New York, Second Edition, 1130 pp.
- LORD RAYLEIGH, 1880: On the Stability of Certain Fluid Motions. Scientific Papers, vol. I, 474-487. Dover Publ. Inc., New York, N.Y.
- MOURA, A.D., 1975: The Eigensolutions of the Linearized balance equations over a sphere. Submitted to J.Atmos.Sci. for publication.
- OORT, A.H. and E.M. RASMUSSEN, 1971: Atmospheric circulation statistics. NOAA Prof. Paper 5, 323 pp.
- PEDLOSKY, J., 1964.a: The stability of currents in the atmosphere and the ocean: Part I. J.Atmos.Sci., 21, 201-219.
- PEDLOSKY, J., 1964.b: The stability of currents in the atmosphere and the ocean: Part II. J.Atmos.Sci., 21, 342-353.
- PHILLIPS, N.A., 1954: Energy transformations and meridional circulations associated with simple baroclinic waves in a two-level, quasi-geostrophic model. Tellus, 6, 273-286.
- SIMMONS, A.J., 1974: The meridional scale of baroclinic waves. J.Atmos.Sci., 31, 1515-1525.
- STONE, P.H., 1969: The meridional structure of baroclinic waves. J.Atmos.Sci., 26, 376-389.
- STONE, P.H., 1974: The meridional variation of the eddy heat fluxes by baroclinic waves and their parameterization. J.Atmos.Sci., 31, 444-456.

FIGURE LEGENDS

Fig. 1 - Members of the family of shear profiles $\bar{U}_1 - \bar{U}_3 = 4\Omega a \Lambda \cos(\text{lat})(1 + \delta \sin^2(\text{lat}))$ used for the solutions far from neutral stability. The local baroclinic stability criterion $4\Omega a S \cos(\text{lat})/\sin^2(\text{lat})$ for $S = 0.005$ and the observed mean annual values of \bar{U} (200 mb) - \bar{U} (700 mb) (Oort and Rasmusson, 1971) are also shown.

Fig. 2 - Members of the family of shear profiles $\bar{U}_1 - \bar{U}_3 = 4\Omega a \Lambda \cos(\text{lat})(1 + \delta \sin^2(\text{lat}))$ used for the solutions near neutral stability. The local baroclinic stability criterion $4\Omega a S \cos(\text{lat})/\sin^2(\text{lat})$ for $S = 0.005$ and the observed mean annual values of \bar{U} (200 mb) - \bar{U} (700 mb) (Oort and Rasmusson, 1971) are also shown.

Fig. 3a - Eigenfunctions ϕ_1' and ϕ_3' for the most unstable mode for the profile 2 (Fig. 1). Numerical values of the parameters are: $S = 0.005$; $\omega = \Lambda = 0.01$; $\delta = 0$. This mode has $\sigma = -0.03132 + i 0.008424$; $s = 4$; $m = 3$; $\text{SYM} = 0$ (Symmetric streamfunction).

Fig. 3b - Angular momentum and heat transports corresponding to Fig. 3a.

Fig. 4a - Eigenfunctions ϕ_1' and ϕ_3' for the most unstable mode for the profile 2 (Fig. 2). Numerical values of the parameters are: $S = 0.005$; $\omega = \Lambda = 0.006$; $\delta = 0$. This mode has $\sigma = -0.01055 + i 0.0007142$; $s = 2$; $m = 5$; $\text{SYM} = 0$.

Fig. 4b - Angular momentum and heat transports corresponding to Fig. 4a.

Fig. 5a - Eigenfunctions ϕ_1' and ϕ_3' for the most unstable mode for the profile 3 (Fig. 1). Numerical values of the parameters are: $S = 0.005$; $\omega = \Lambda = 0.007$; $\delta = 2$. This mode has $\sigma = 0.009452 + i 0.01809$; $s = 4$; $m = 4$; $\text{SYM} = 0$.

Fig. 5b - Angular momentum and heat transports corresponding to Fig. 5a.

Fig. 6a - Eigenfunctions ϕ_1' and ϕ_3' for the most unstable mode for the profile 3 (Fig. 2). Numerical values of the parameters are: $S = 0.005$; $\omega = \Lambda = 0.002$; $\delta = 2$. This mode has $\sigma = -0.003585 + i 0.0003503$; $s = 2$; $m = 5$; $\text{SYM} = 0$.

Fig. 6b - Angular momentum and heat transports corresponding to Fig. 6a.

Fig. 7a - Same as Fig. 5a, but for the profile 4 (Fig. 1); $S = 0.005$; $\omega = \Lambda = 0.025$; $\delta = -1$. $\sigma = -0.1210 + i 0.01267$; $s = 5$; $m = 2$; $\text{SYM} = 0$.

Fig. 7b - Angular momentum and heat transports corresponding to Fig. 7a.

Fig. 8a - Same as Fig. 5a, but for the profile 4 (Fig. 2); $S = 0.005$; $\omega = \Lambda = 0.02$; $\delta = -1$. $\sigma = -0.1087 + i 0.0004115$; $s = 5$; $m = 2$; $\text{SYM} = 0$.

Fig. 8b - Angular momentum and heat transports corresponding to Fig. 8a.

Fig. 9a - Same as Fig. 5a, but for the profile 5 (Fig. 1); $S = 0.005$;
 $\omega = \Lambda = -0.001$; $\delta = -28$. $\sigma = 0.04293 + i 0.02188$; $s = 3$; $m = 4$;
SYM = 1 (Antisymmetric streamfunction).

Fig. 9b - Angular momentum and heat transports corresponding to Fig. 9a.

Fig. 10a - Same as Fig. 6a, but for the profile 3 (Fig. 2 with shear
coordinate decreased by a factor of 4). $S = 0.00125$; $\omega = \Lambda = 0.0005$;
 $\delta = 2$. $\sigma = -0.16 + i 0.00026$; $s = 4$; $m = 11$; SYM = 1.

Fig. 10b - Angular momentum and heat transports corresponding to Fig. 10a.

Fig. 11a - Same as Fig. 7a, but for the profile 4 (Fig. 1 with shear
coordinate decreased by a factor of 4); $S = 0.00125$; $\omega = \Lambda = 0.00625$;
 $\delta = -1$. $\sigma = -0.0631 + i 0.00725$; $s = 11$; $m = 3$; SYM = 0.

Fig. 11b - Angular momentum and heat transports corresponding to Fig. 11a.

Fig. 12a - Same as Fig. 9a, but for the profile 5 (Fig. 1 with shear
coordinate decreased by a factor of 4); $S = 0.00125$; $\omega = \Lambda = -0.00025$;
 $\delta = -28$. $\sigma = 0.02617 + i 0.01362$; $s = 7$; $m = 10$; SYM = 0.

Fig. 12b - Angular momentum and heat transports corresponding to Fig. 12a.

Table I - Location of important features of the most unstable solutions.

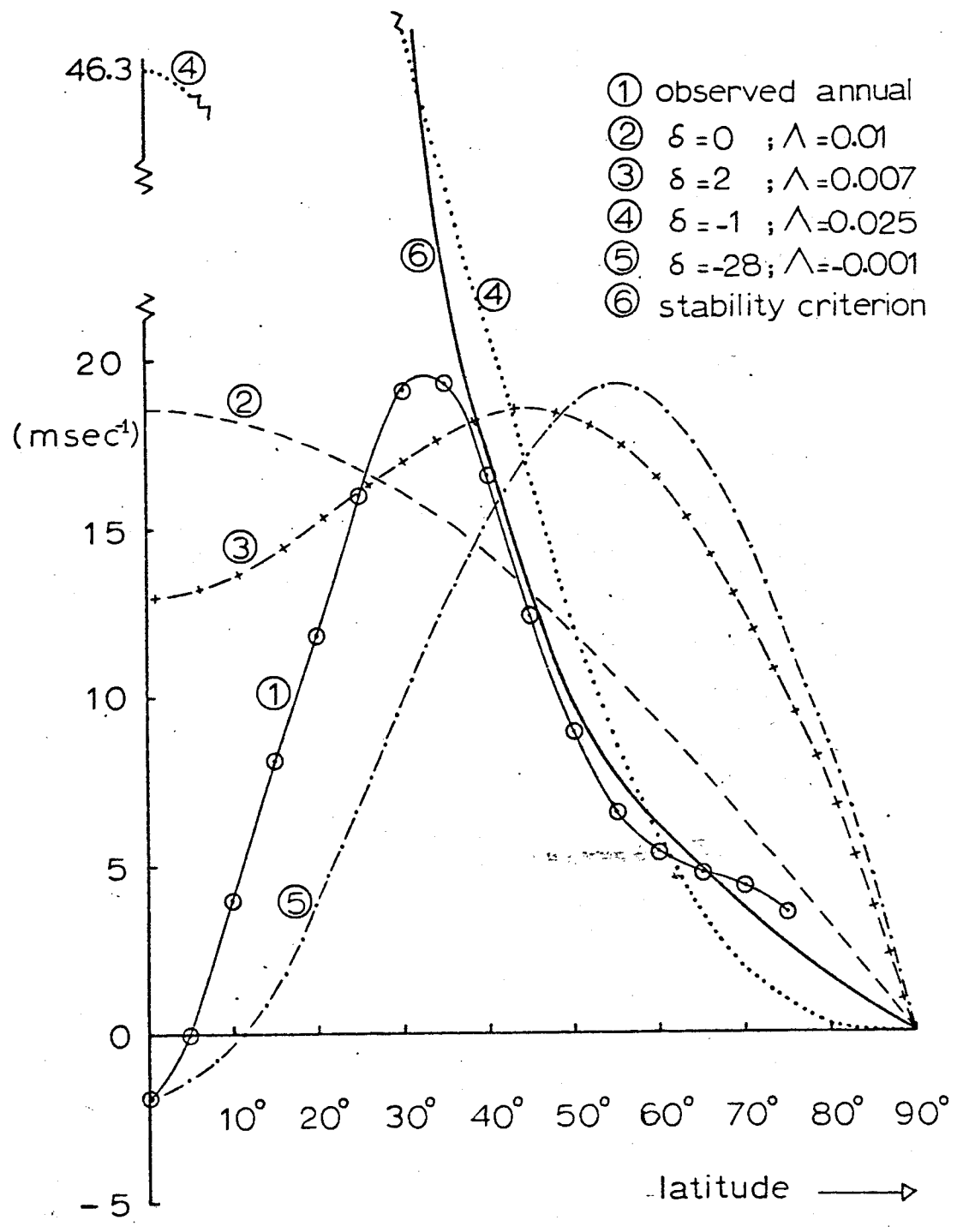


Fig. 1

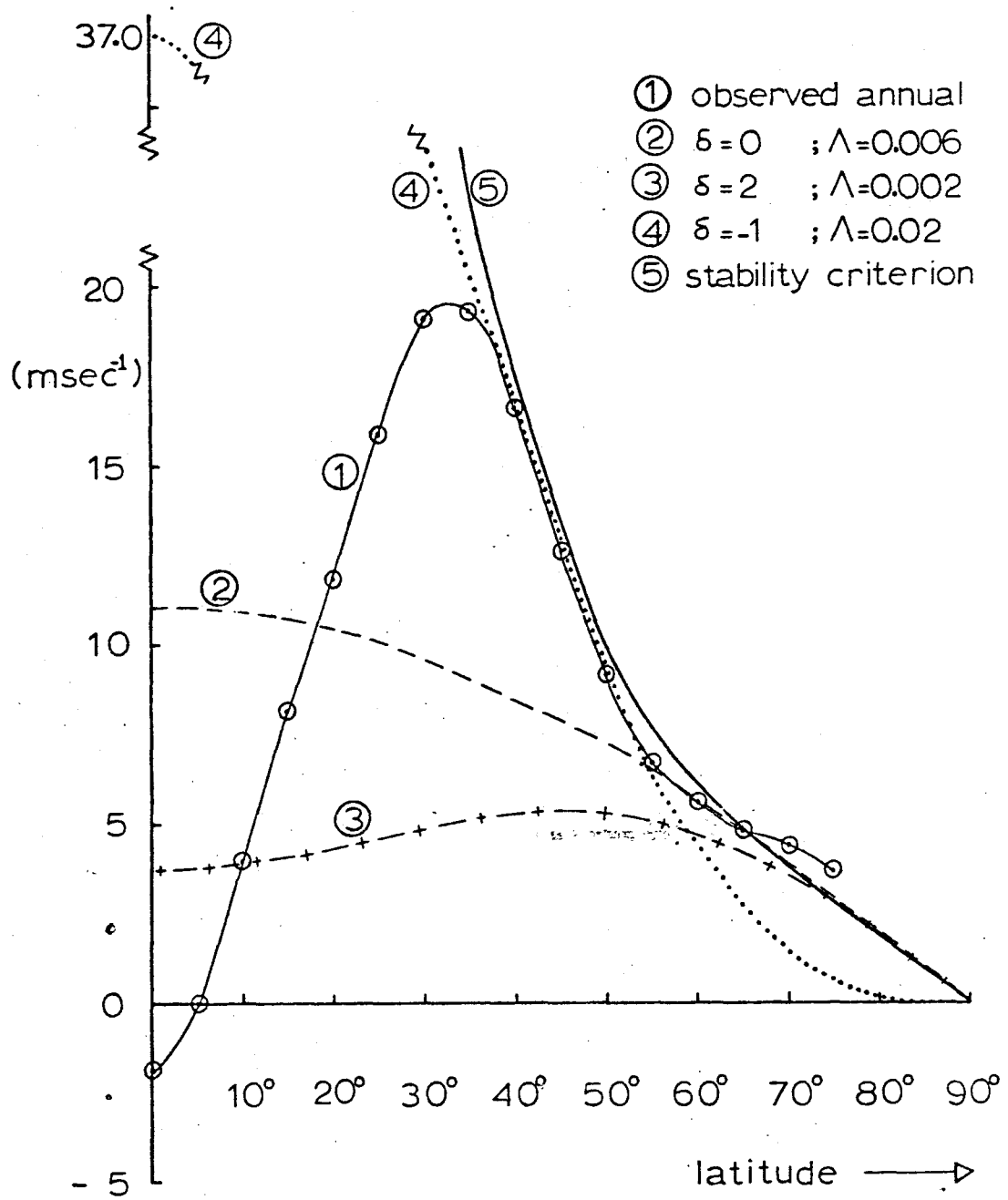


Fig. 2

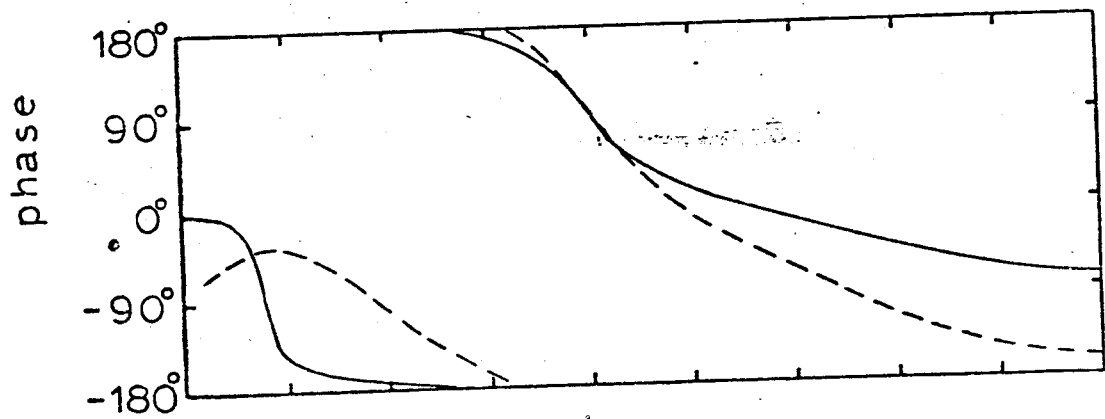
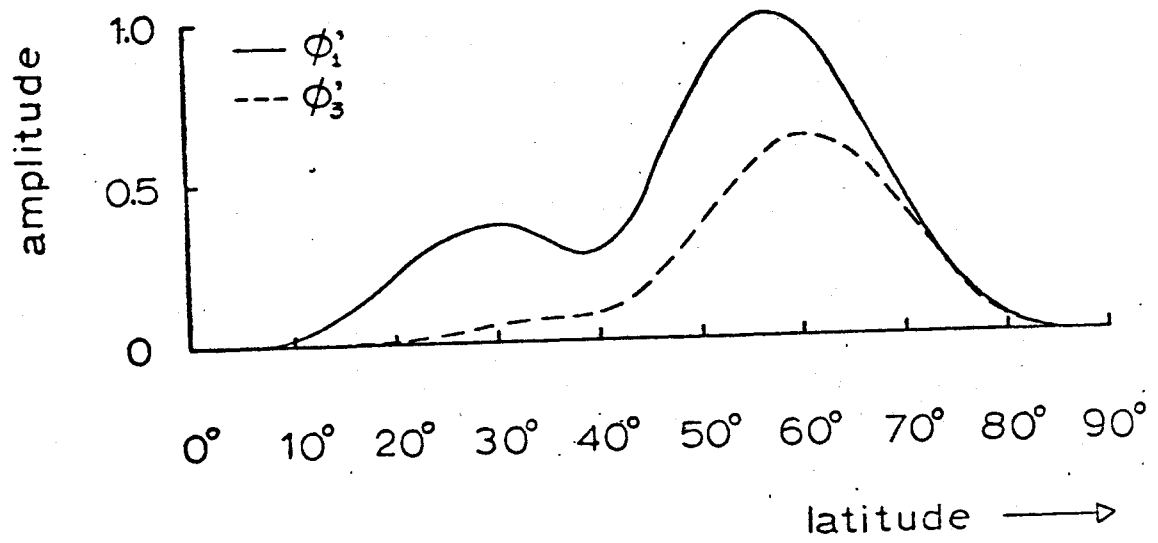


Fig. 3a

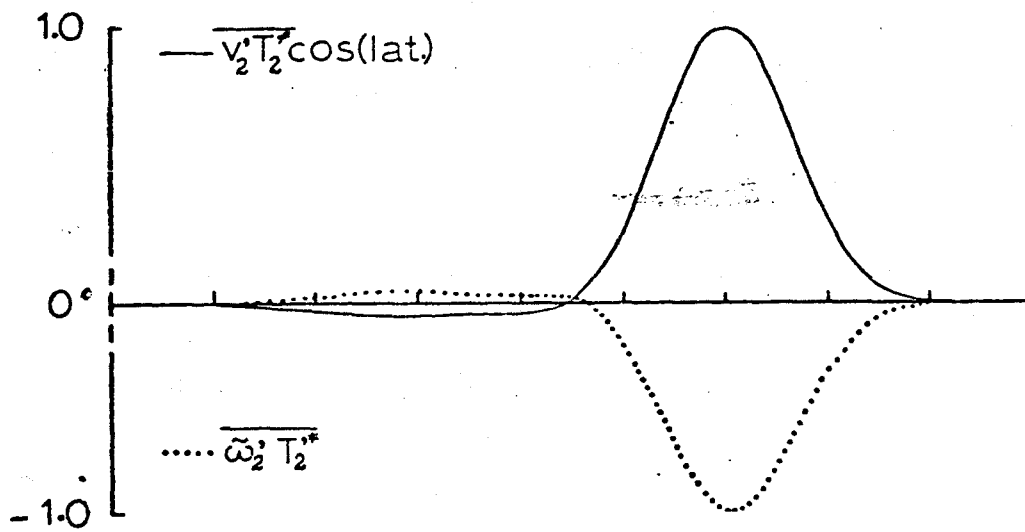
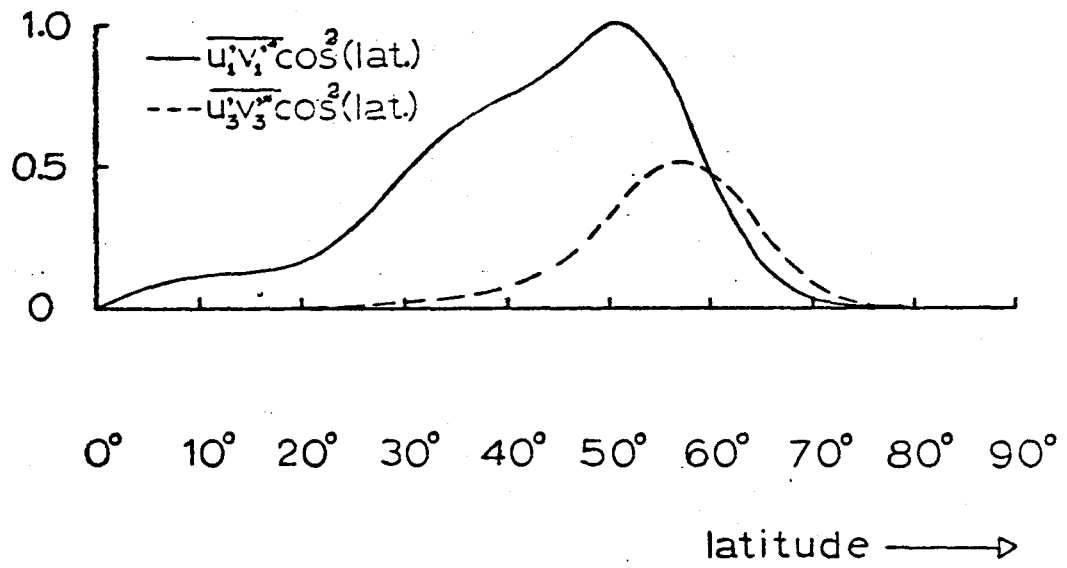


Fig. 3b

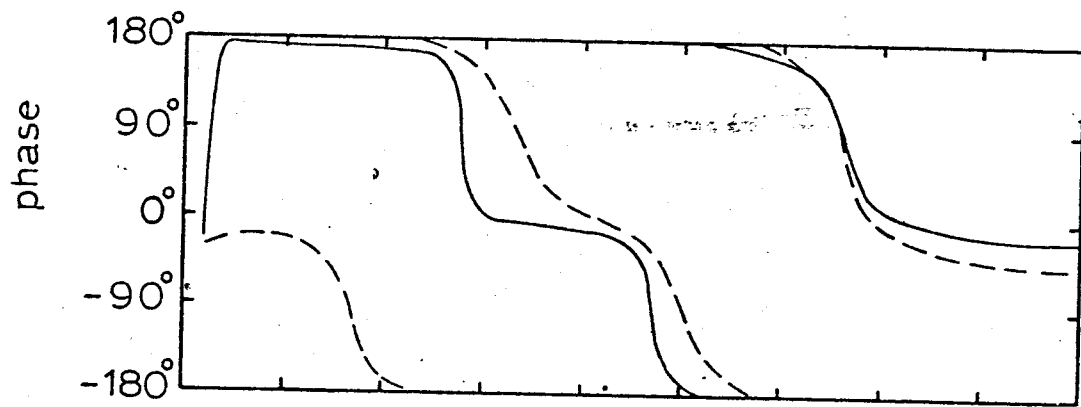
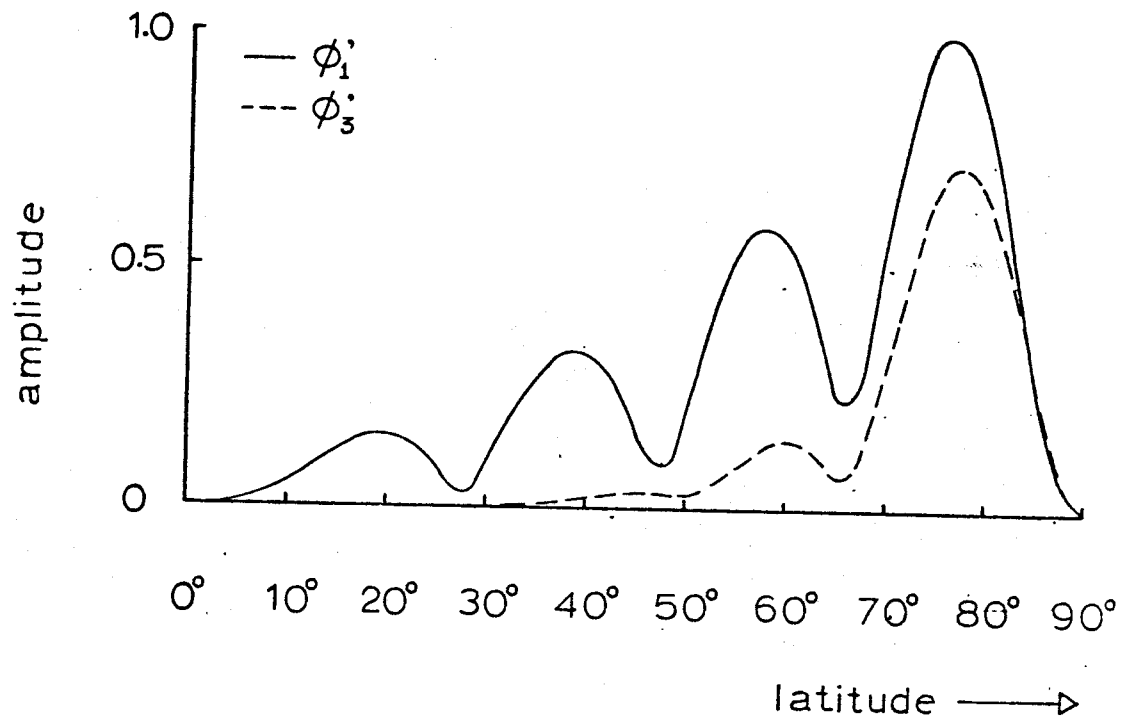


Fig. 4a

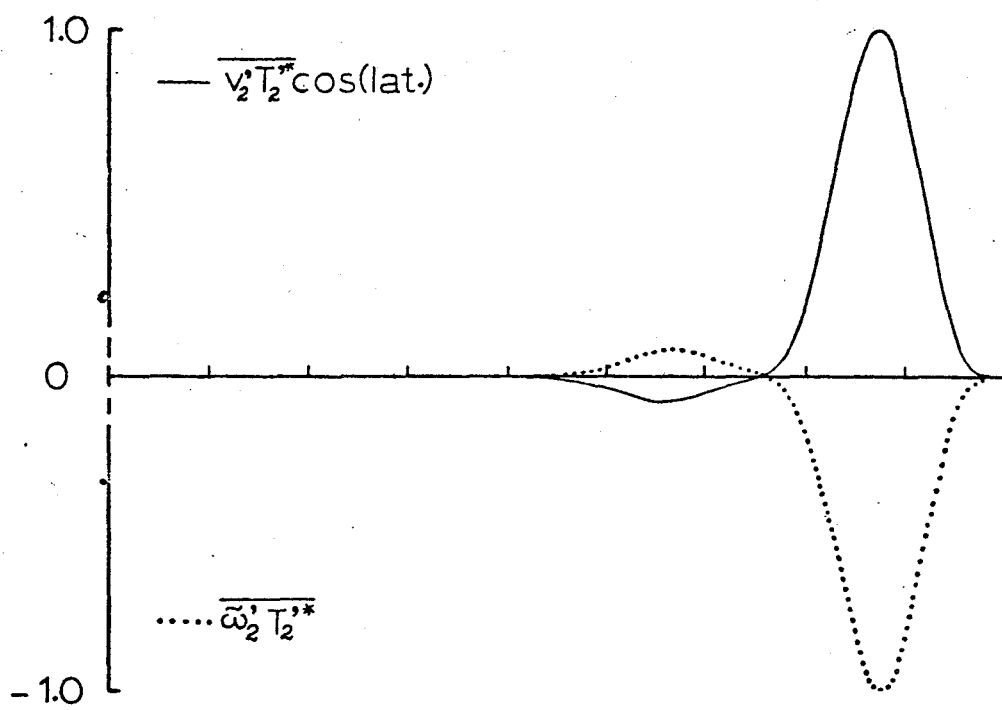
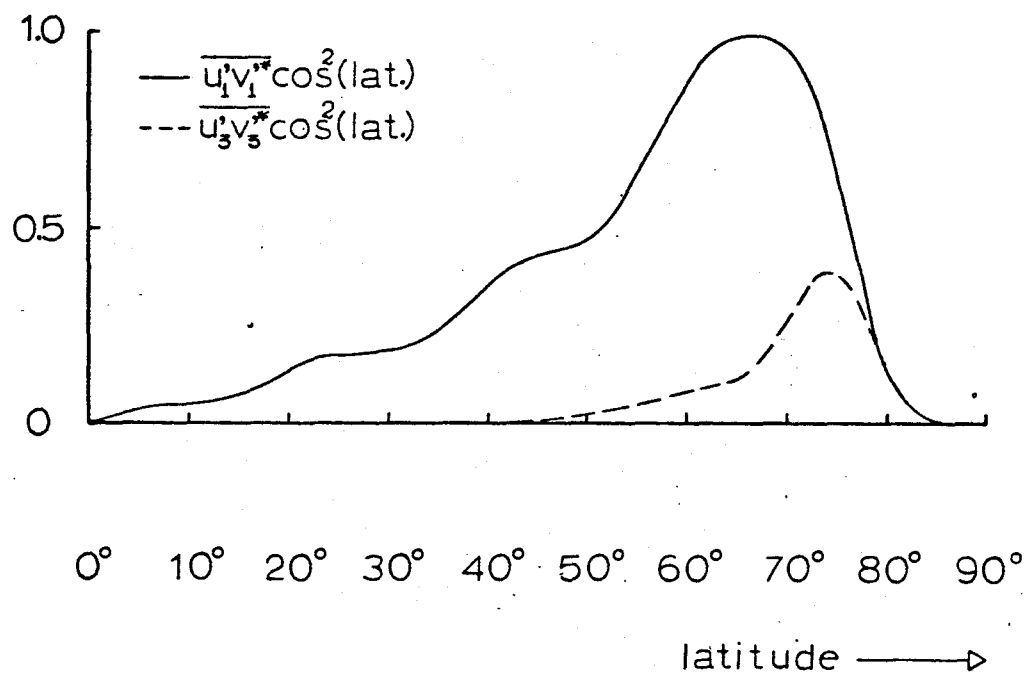


Fig. 4b

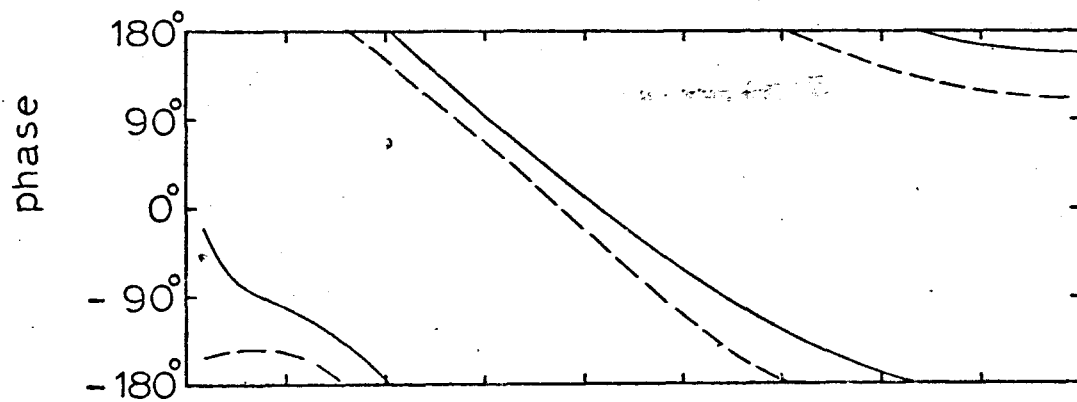
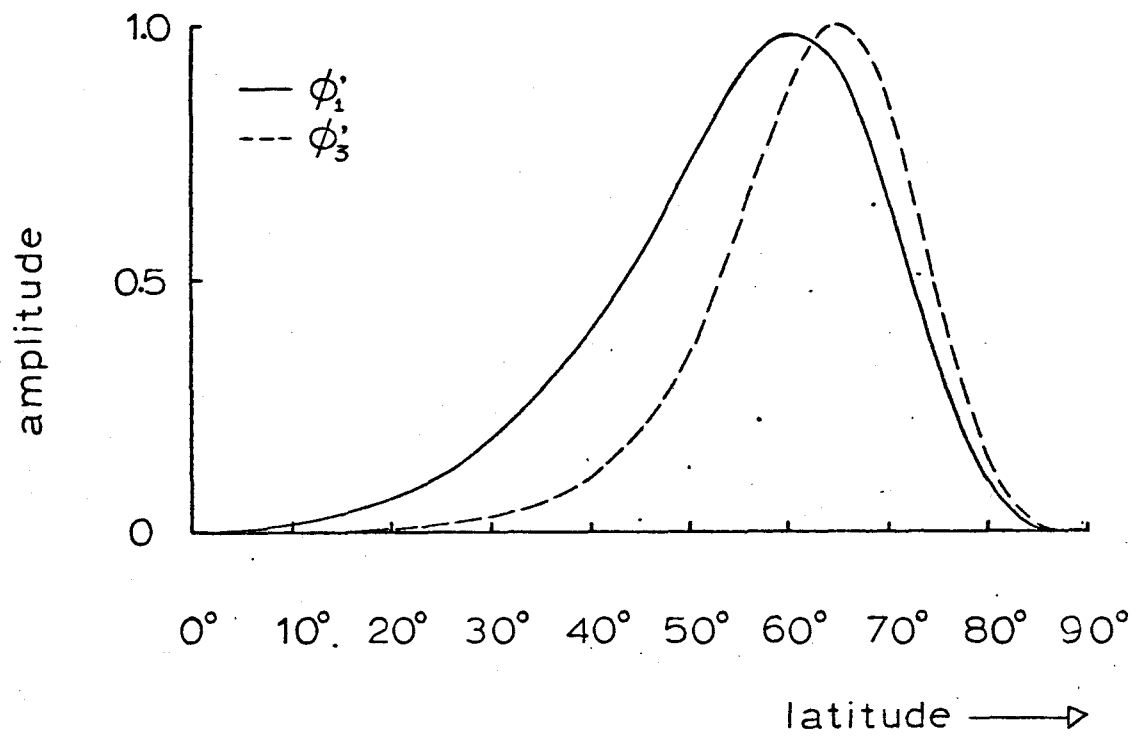


Fig. 5a

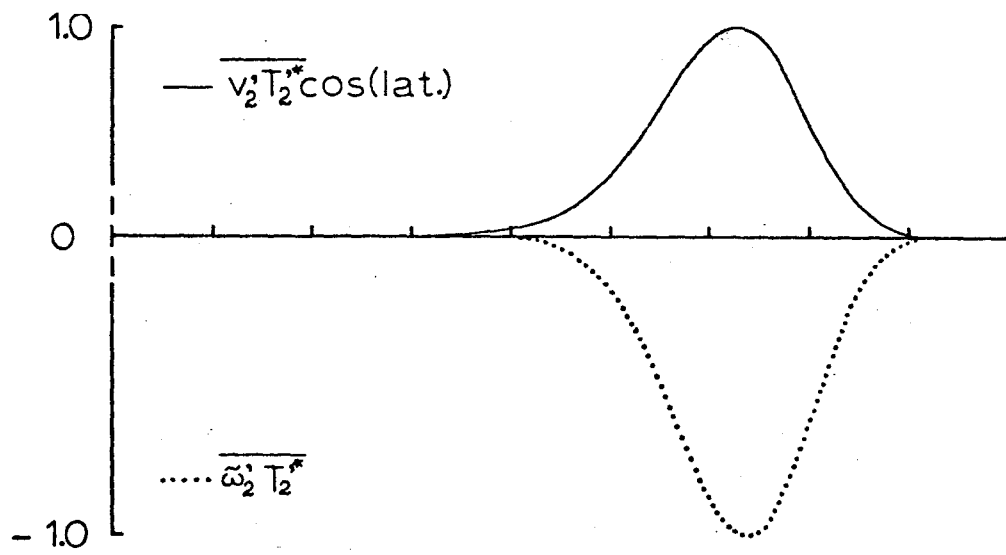
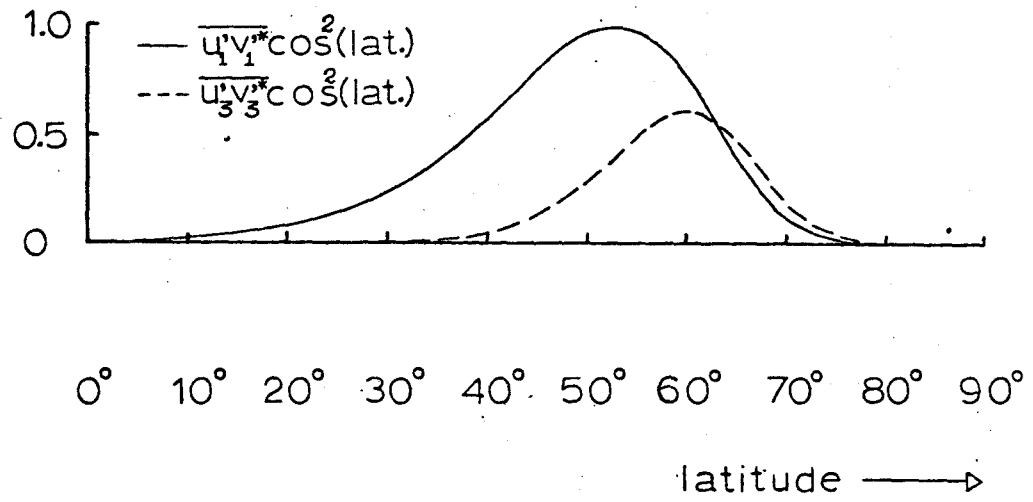


Fig. 5b

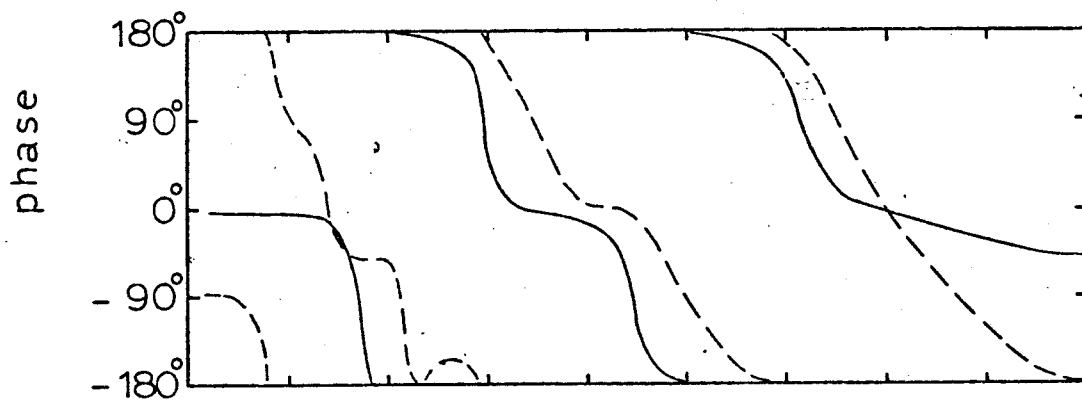
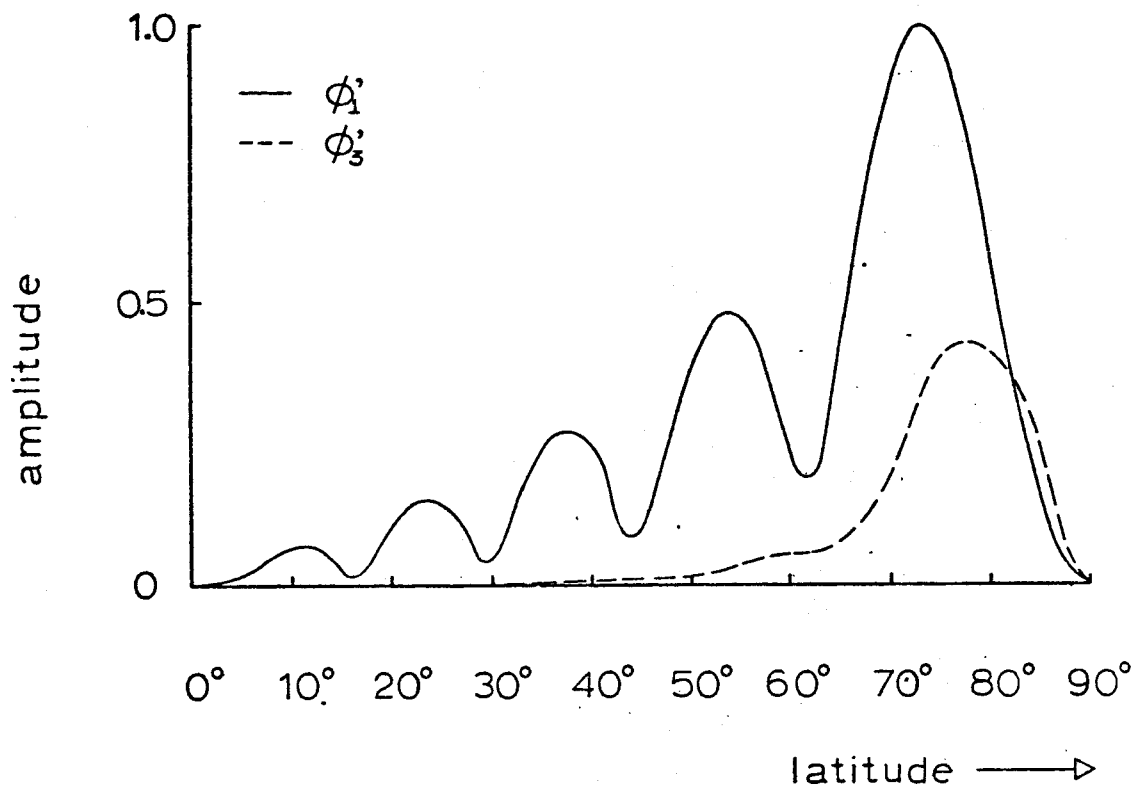


Fig. 6a

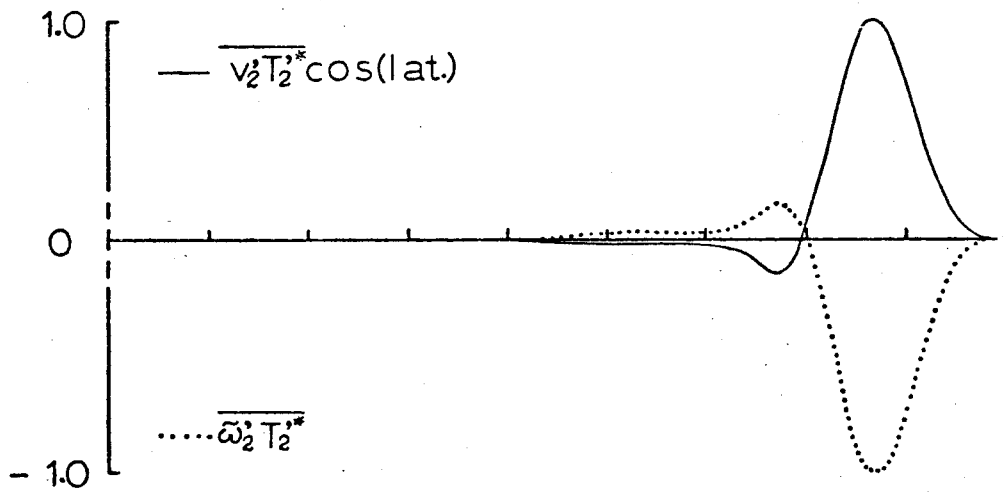
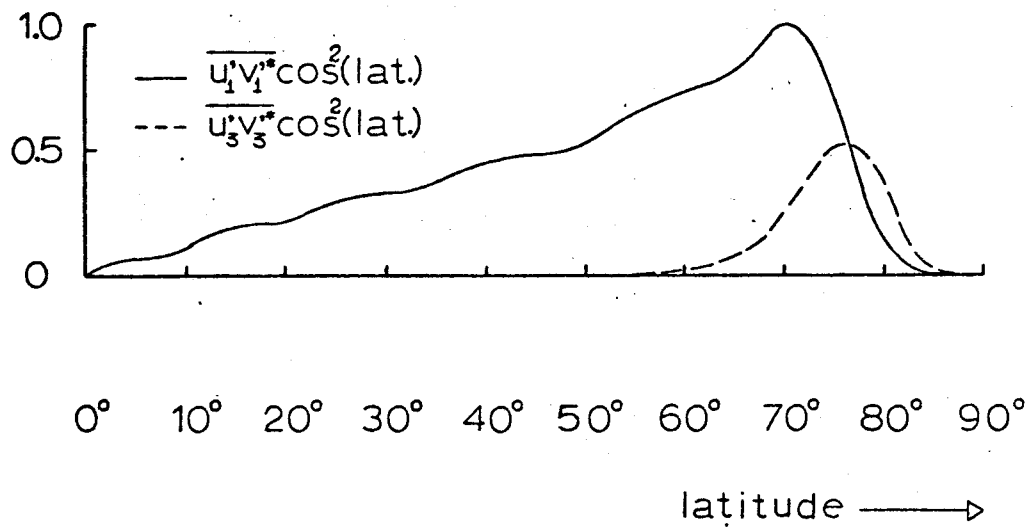


Fig. 6b

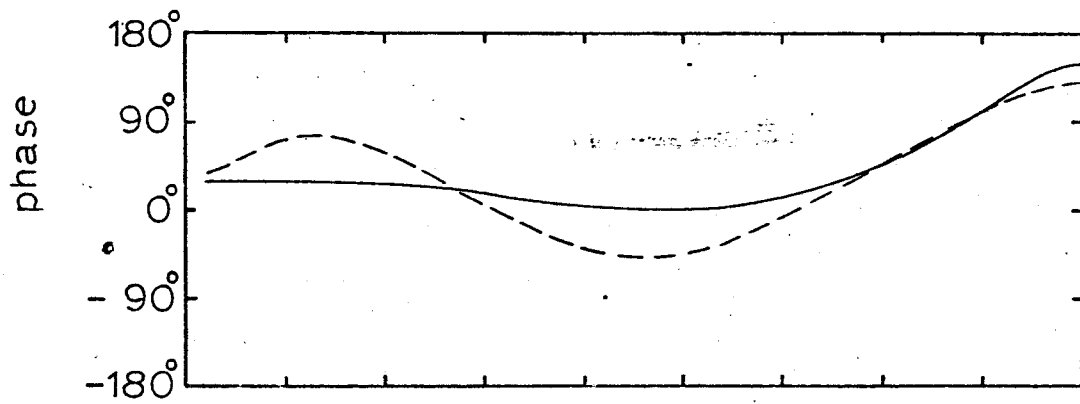
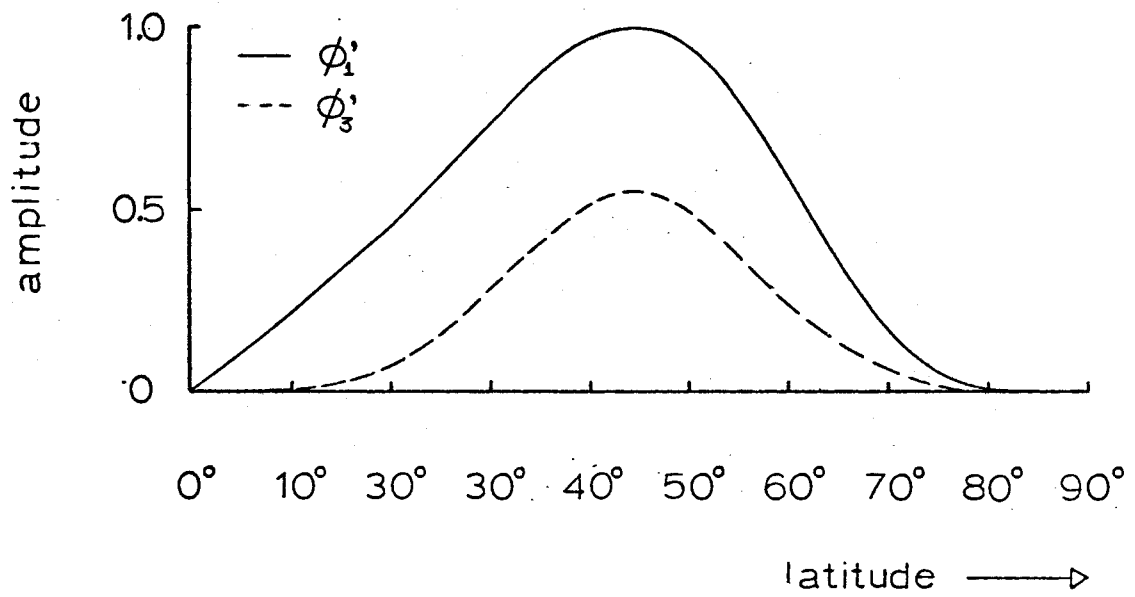


Fig. 7a

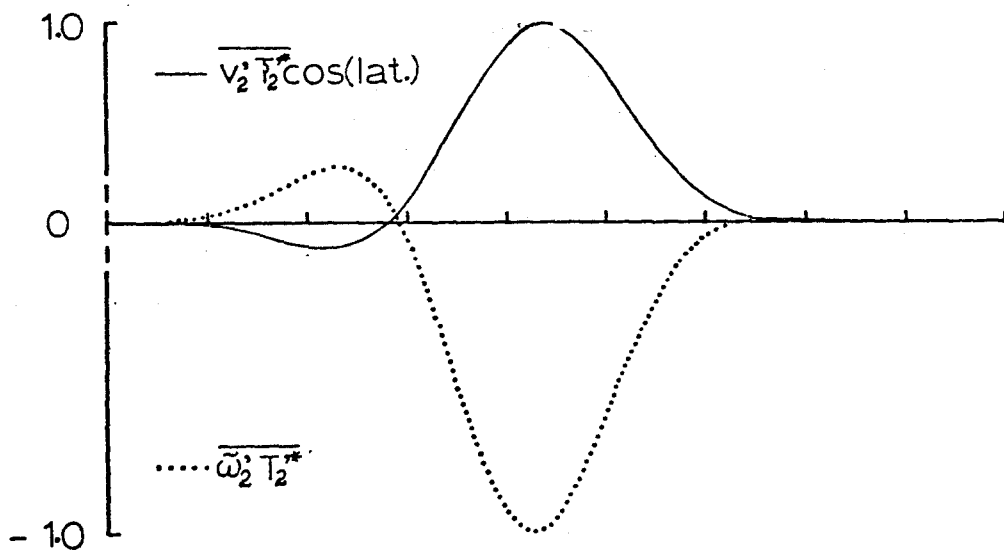
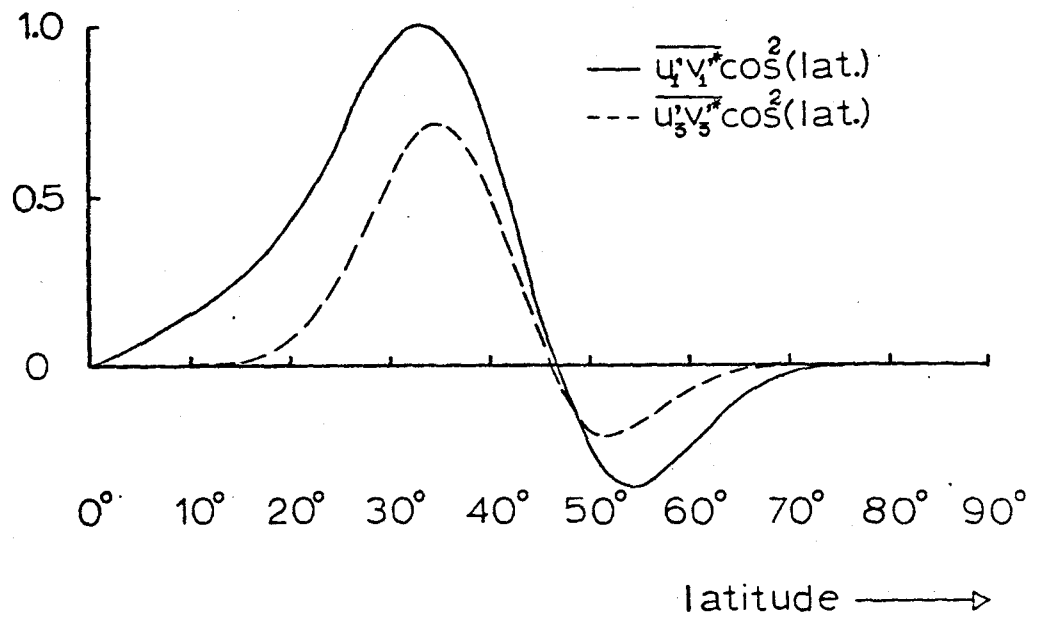


Fig. 7b

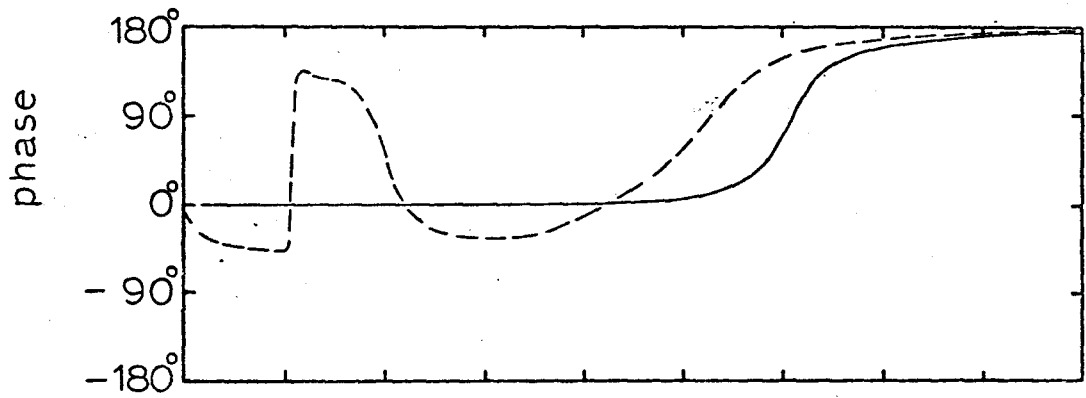
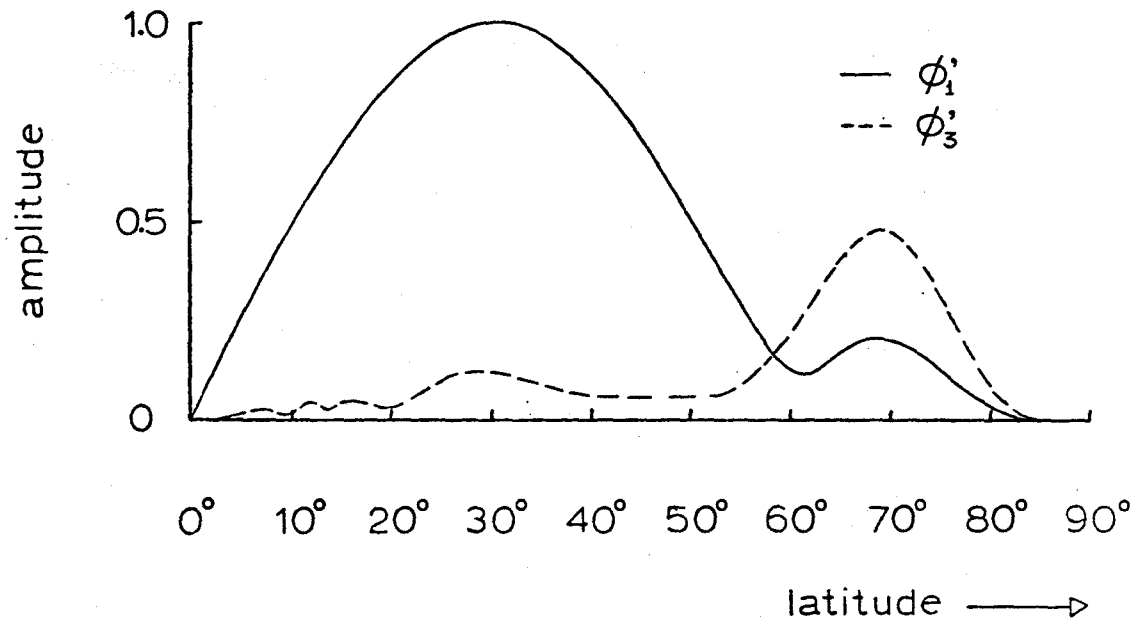


Fig. 8a

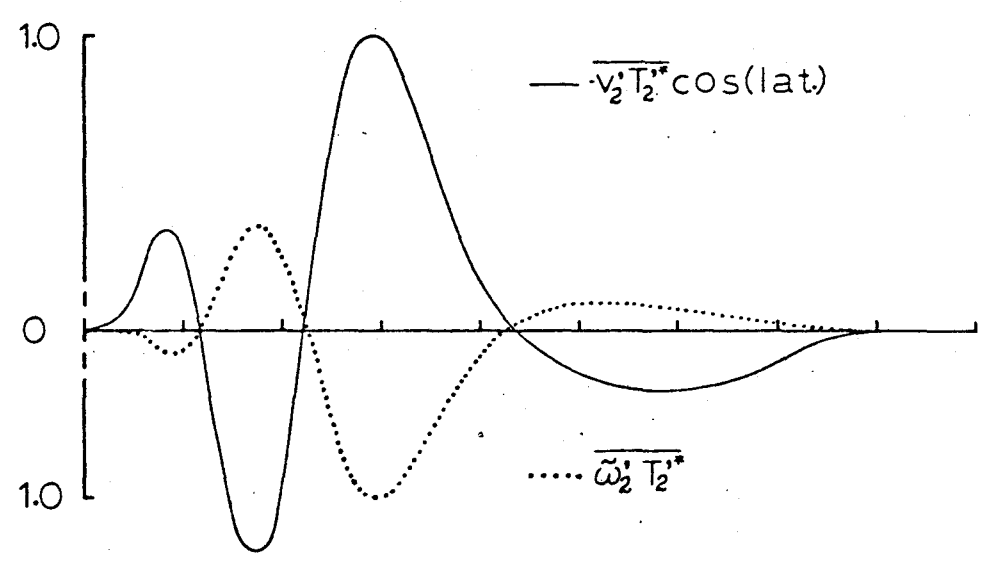
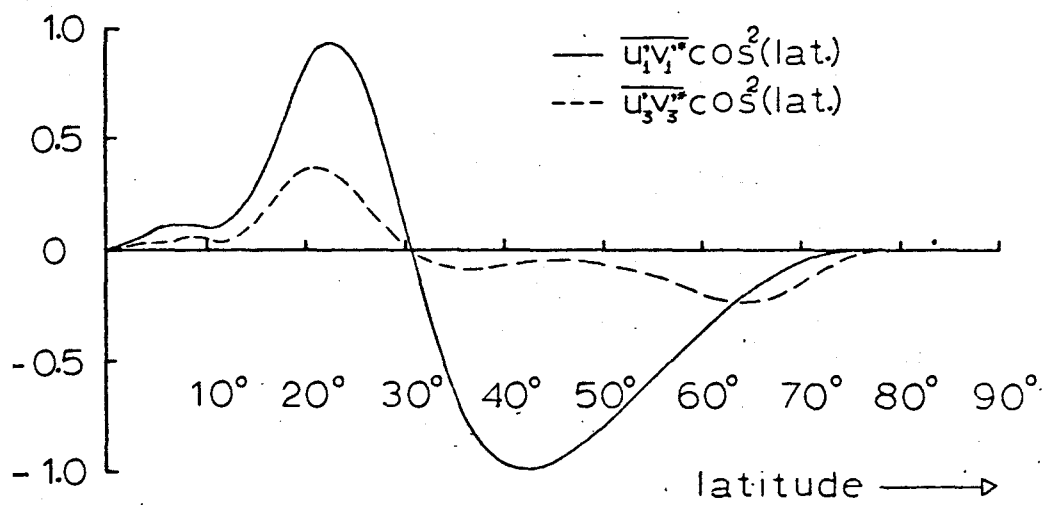


Fig. 8b

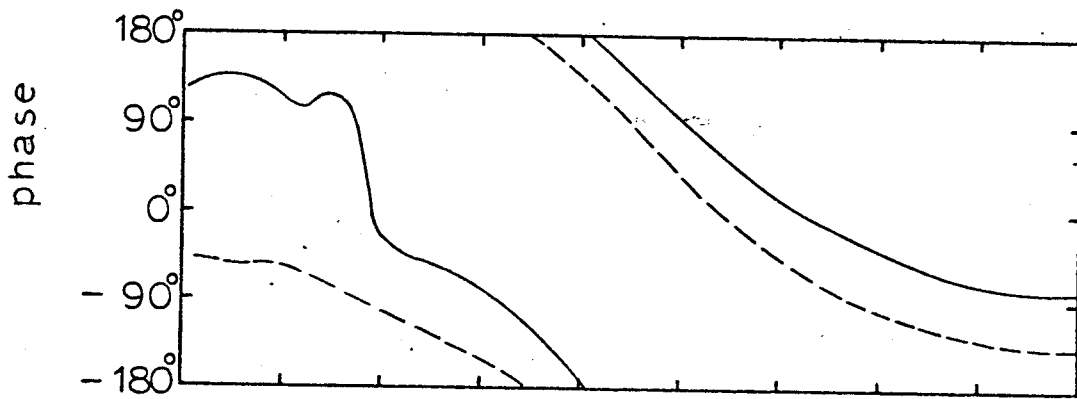
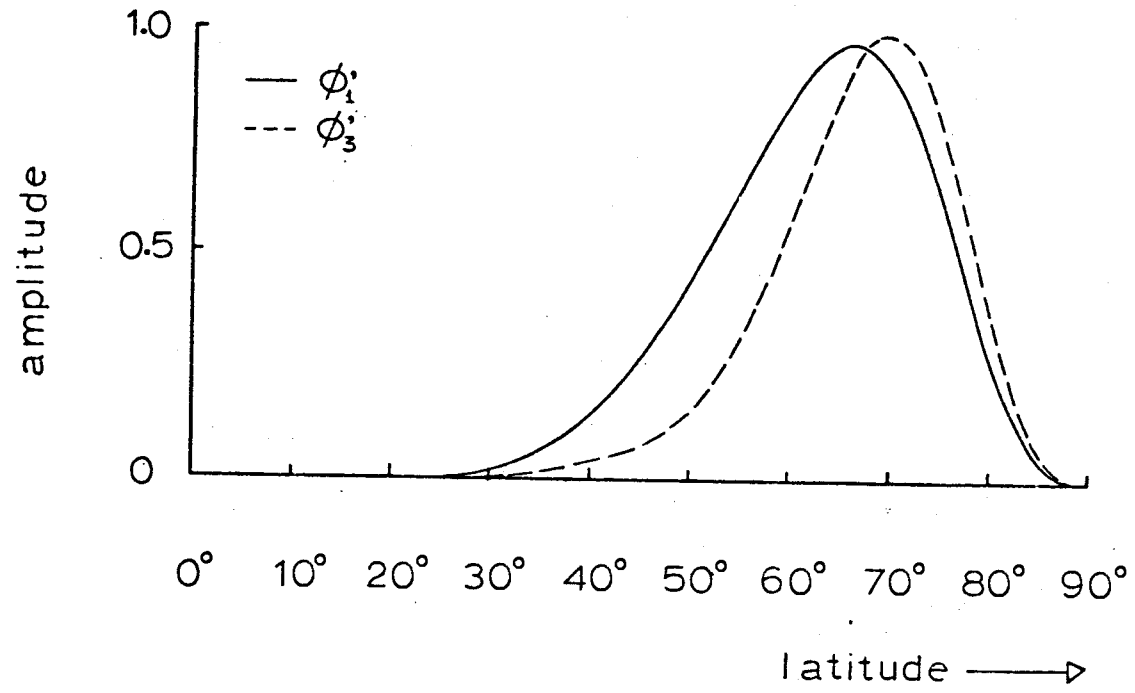


Fig. 9a

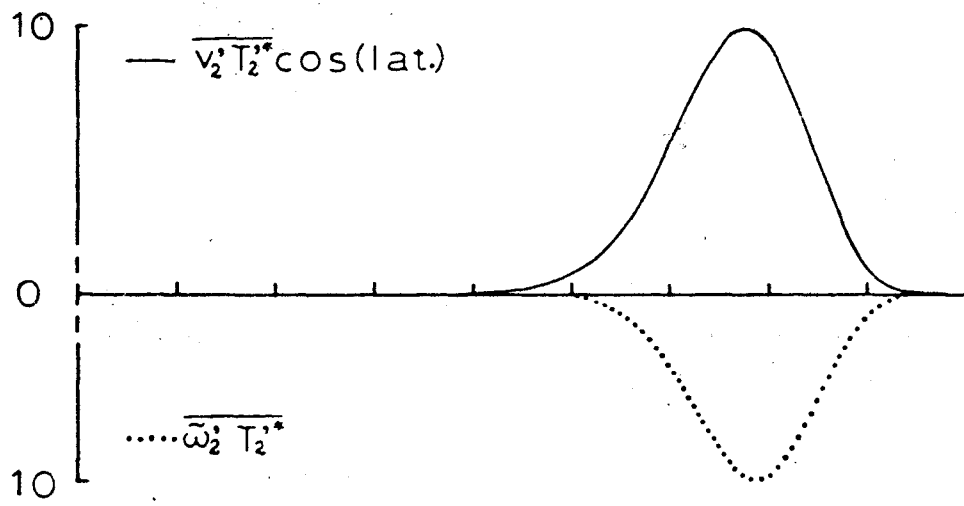
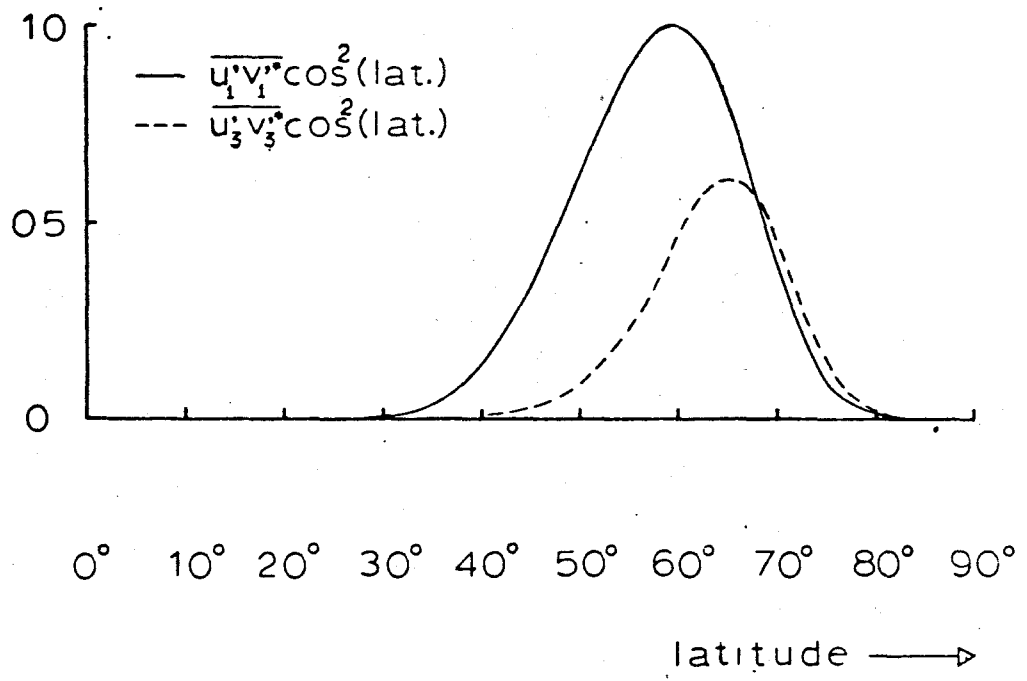


Fig. 9b

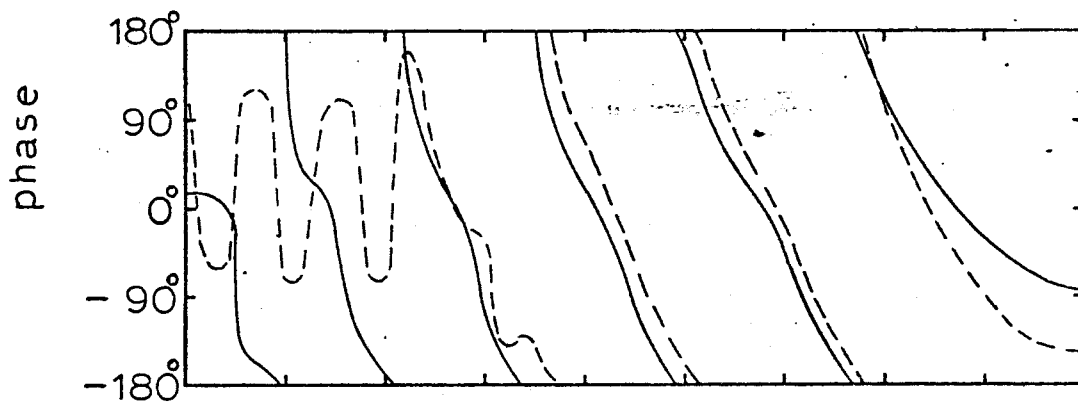
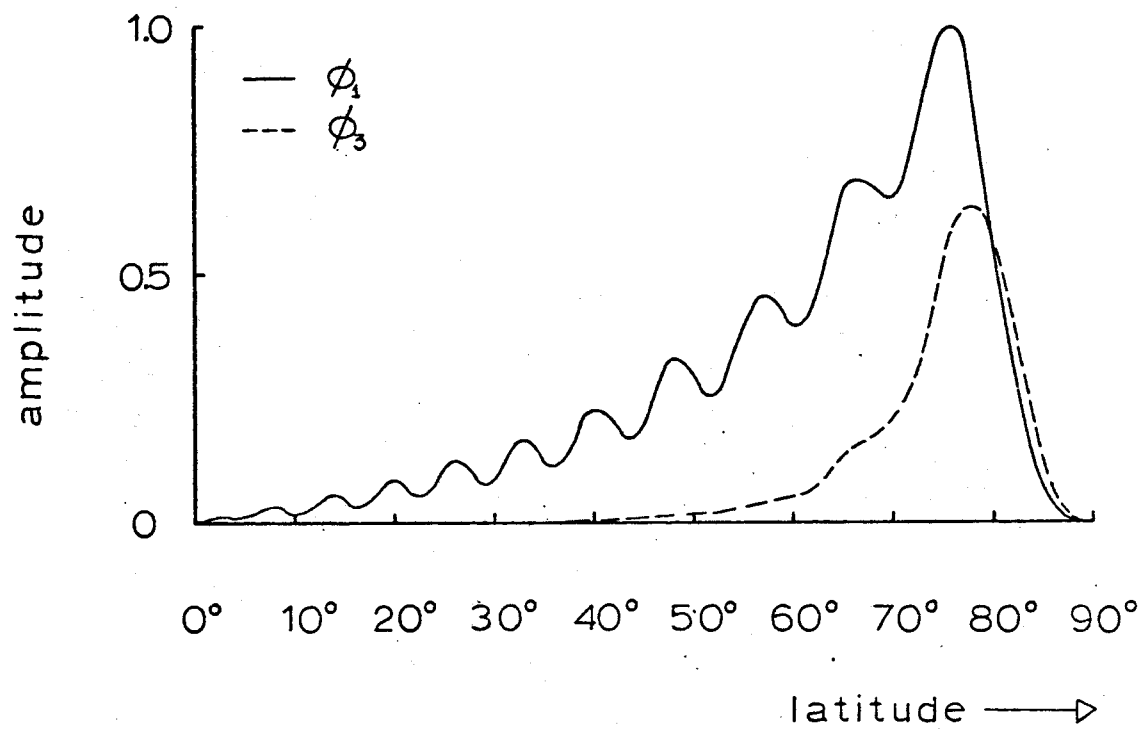


Fig. 10a

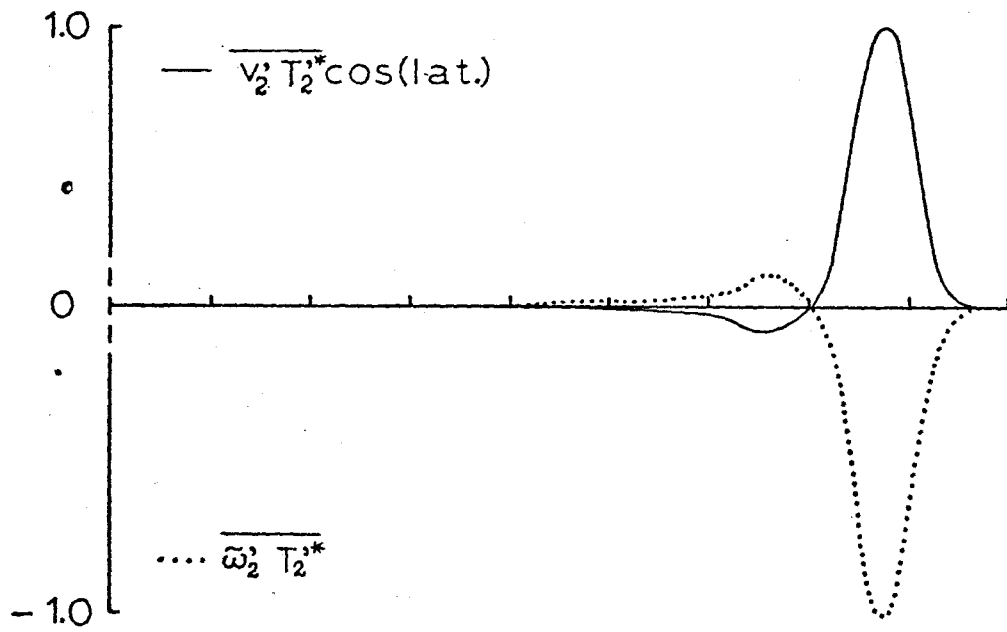
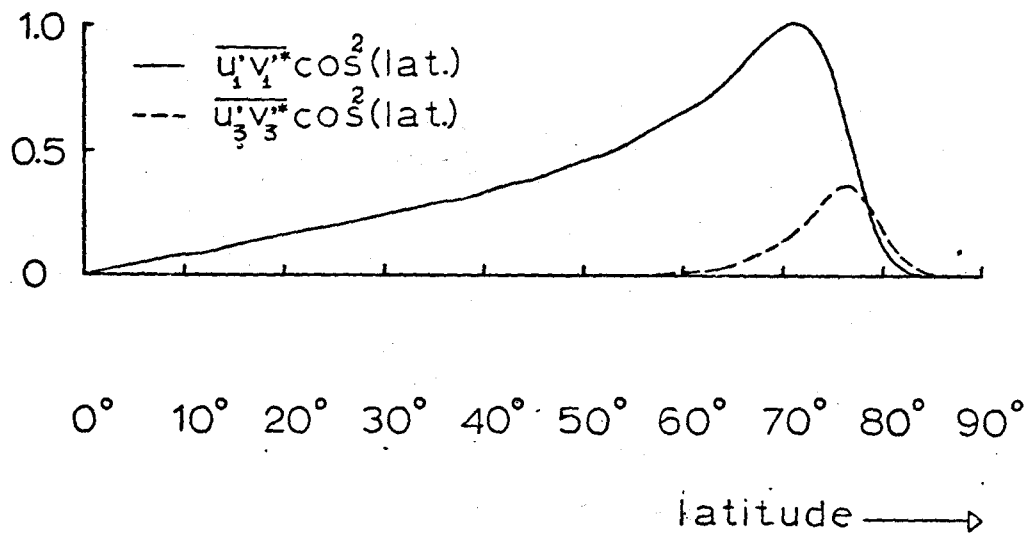


Fig. 10b

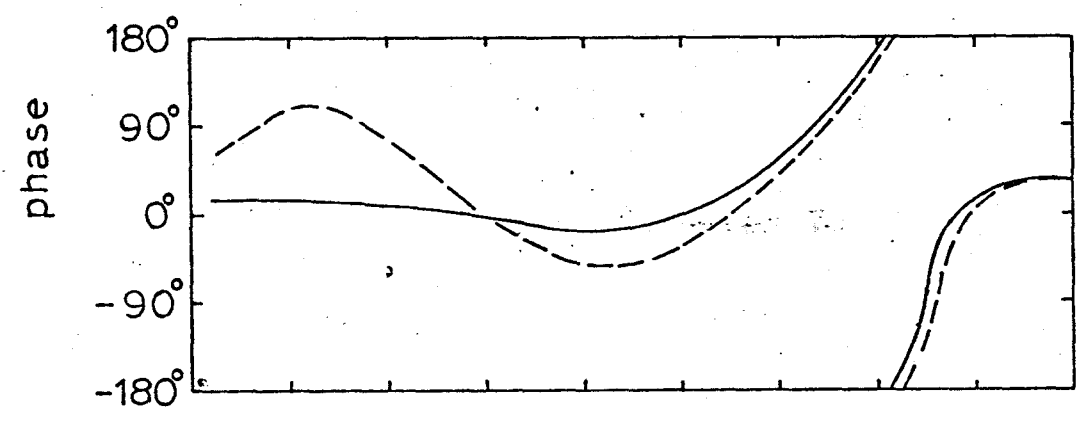
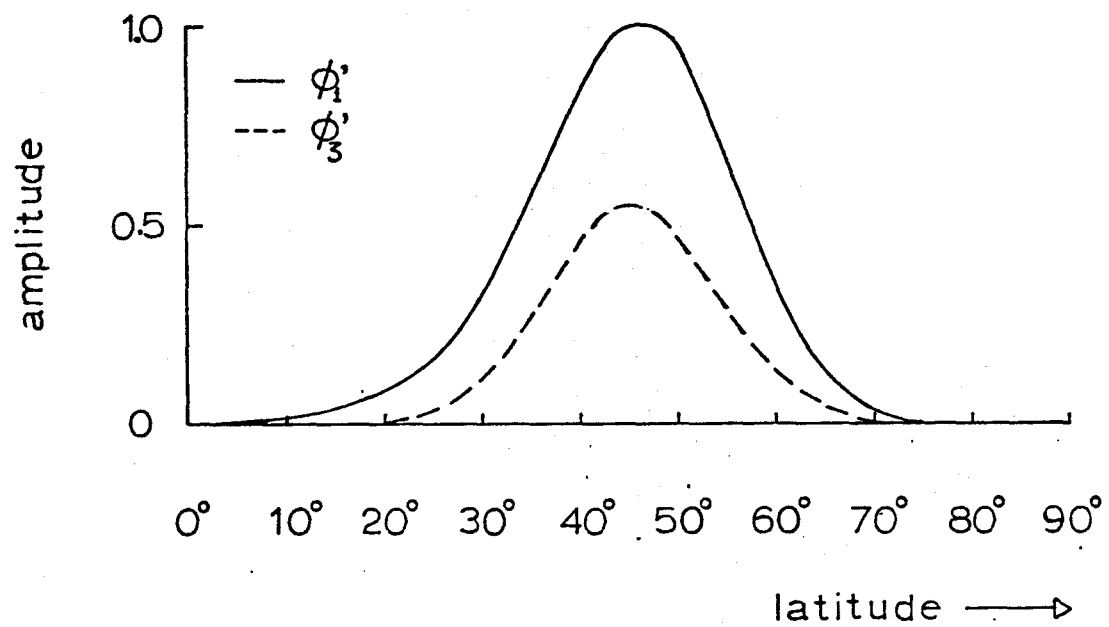


FIG. 11.a

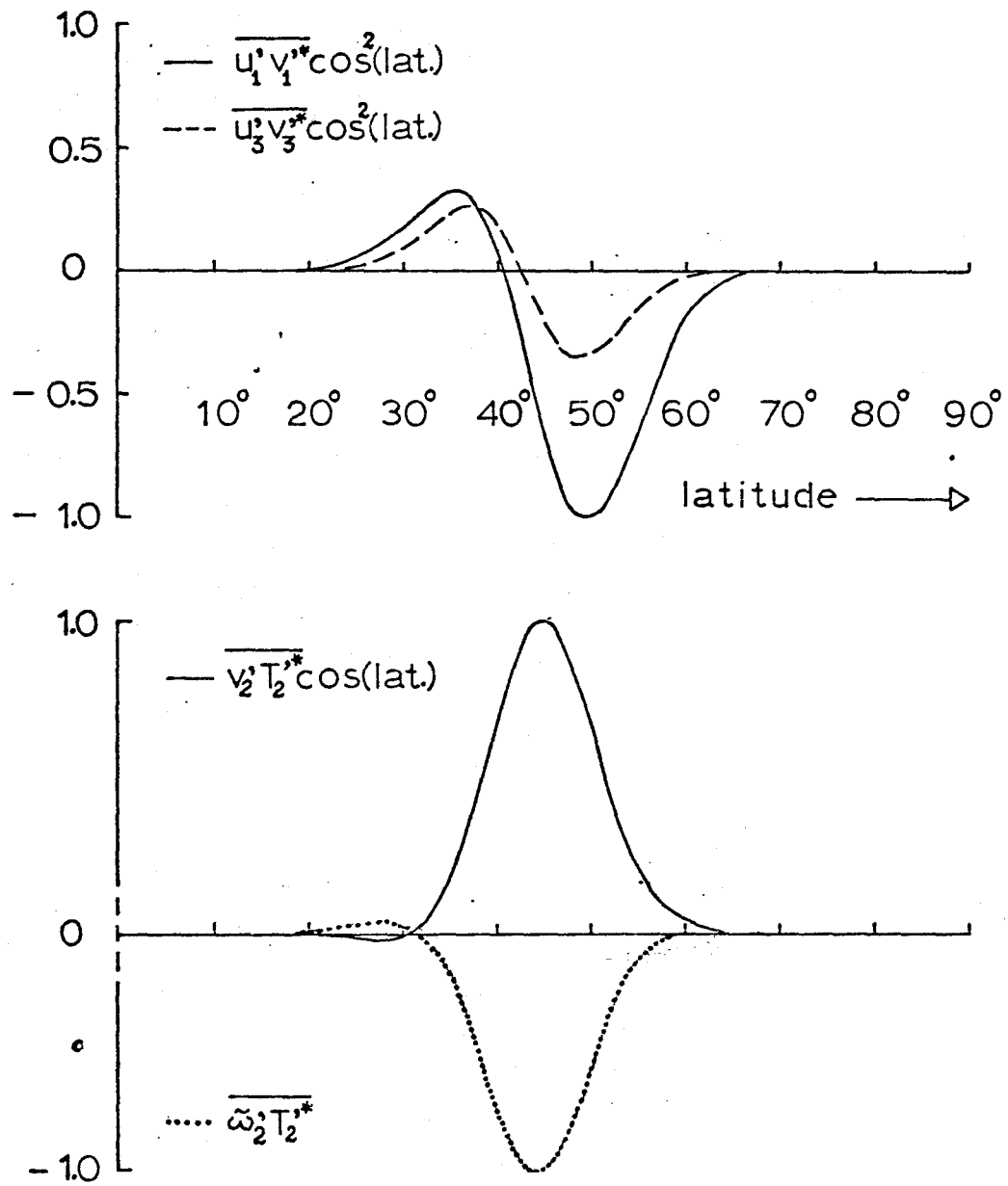


Fig.11.b

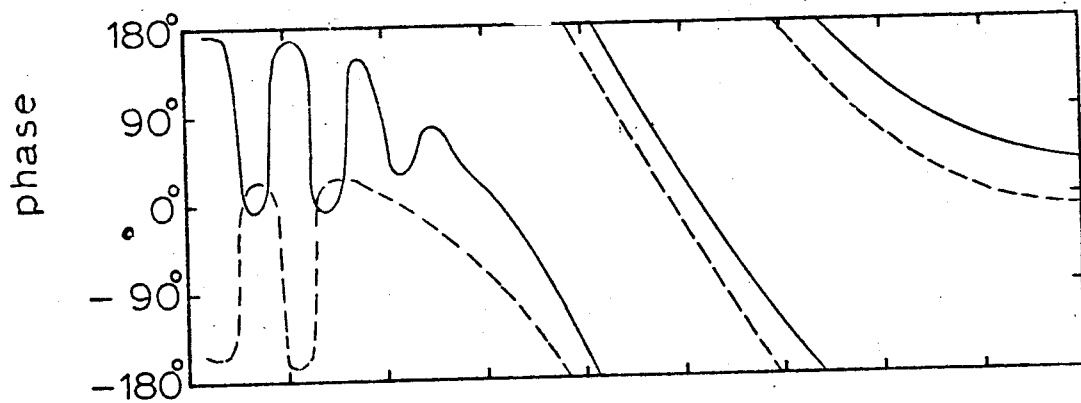
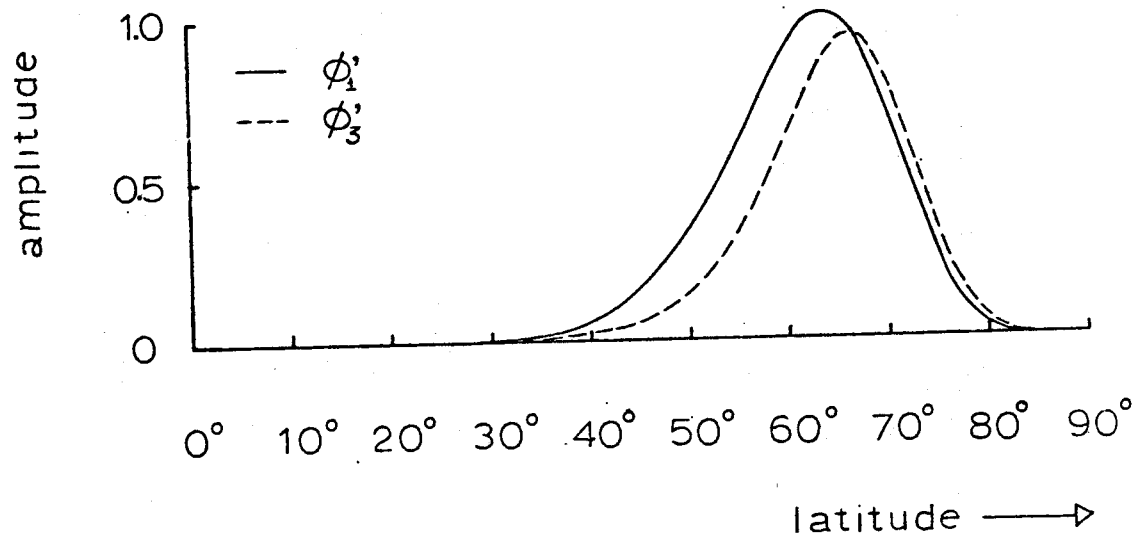


Fig. 12a

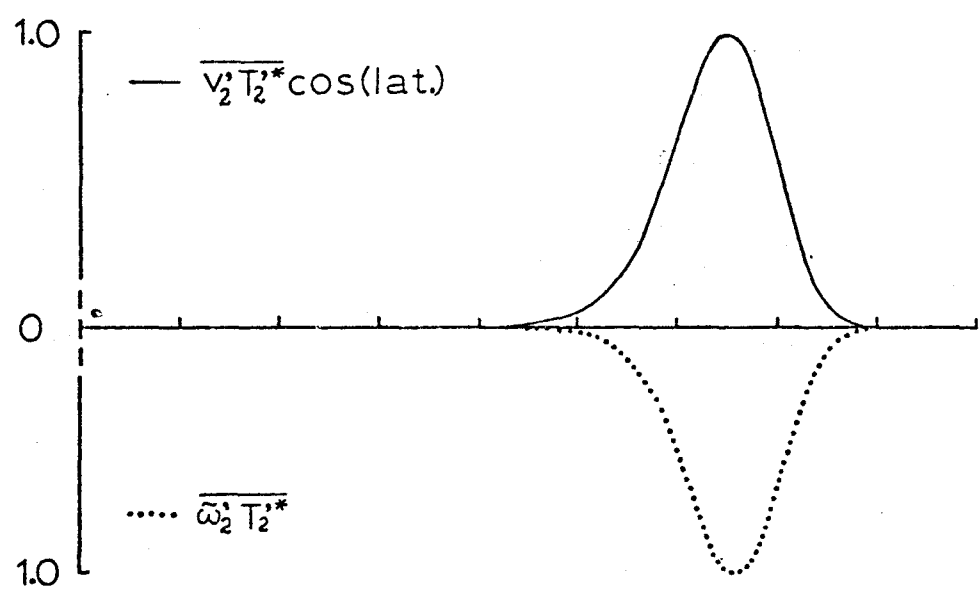
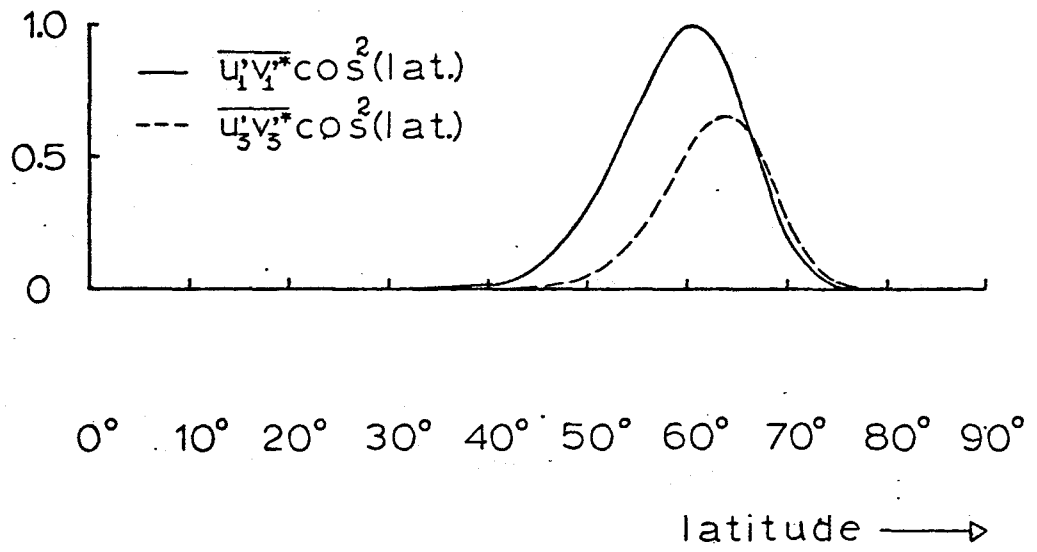


Fig. 12b

Figure no.	Profile no.	Growth rate ν	excess of shear over the local criterion		$ \Phi_1 $	$ \Phi_3 $	$\overline{u_1 v_1^*} (1-\mu^2)$		$\overline{u_3 v_3^*} (1-\mu^2)$		$\overline{v_2 T_2 \mu^{1/2}}$		$\overline{\omega_2 T_2^*}$	
			zero peak	peak			peak	max. flux conv.	peak	max. flux conv.	zero peak	peak	zero peak	peak
3	2 s=.005	.0084	46°	62°	57°	60°	51°	62°	57°	65°	45	10°	46°	61°
5	3 s=.005	.018	40°	61°	60°	65°	53°	64°	60°	68°	—	3°	—	64°
7	4 s=.005	.013	32° (58°)	41°	44°	44°	33° (54°)	44°	35° (52°)	43°	28	14°	29°	43°
9	5 s=.005	.022	42°	63°	66°	70°	60°	68°	65°	72°	—	7°	—	68°
11	4 s=.00125	.00725	32° (58°)	41°	46°	45°	36° (50°)	43°	37° (48°)	44°	31	15°	31°	44°
12	5 s=.00125	.014	42°	63°	64°	67°	61°	67°	64°	68°	—	55°	—	66°
4	2 s=.005	.00071	66°	77°	76°	77°	67°	76°	74°	78°	66	77°	66°	77°
6	3 s=.005	.00035	72°	79°	73°	78°	70°	76°	76°	81°	70	77°	70°	77°
8	4 s=.005	.00041	—	below curve	30°	69°	22° (43°)	31°	21° (64°)	28°	(12°) 22 (43°)	29°	(12°) 22 (43°)	29°
10	3 s=.00125	.00026	72°	79°	76°	78°	71°	77°	76°	80°	70	78°	70°	78°

Table I